# INTEGRATING BIOMECHANICS, HEMODYNAMICS, AND VASCULAR ADAPTATION TO RELATE MECHANISMS OF VASCULAR ADAPTATION TO ARTERIAL PULSATILE PRESSURE IN HEALTH AND DISEASE

A Dissertation

by

PHUC HOANG NGUYEN

Submitted to the Office of Graduate and Professional Studies of
Texas A&M University
in partial fulfillment of the requirements for the degree of

DOCTOR OF PHILOSOPHY

| | |
|---|---|
| Chair of Committee, | Christopher M. Quick |
| Committee Members, | Randolph H. Stewart |
| | John C. Criscione |
| | Ranjeet M. Dongaonkar |
| Head of Department, | John N. Stallone |

August 2014

Major Subject: Biomedical Sciences

## ABSTRACT

The inherent complexity of the mammalian systemic arterial system has presented numerous challenges to relating basic vascular biology to clinically-relevant derangements of blood pressures and flows. The field of biomechanics has identified how local changes in pulsatile blood pressures and flows lead to changes in local endothelial shear stress and circumferential wall stress. The field of mechanobiology has identified how local changes in wall circumferential stress and endothelial shear stress lead to changes in arterial radii, wall thicknesses and stiffnesses. The field of pulsatile hemodynamics has identified how changes in local radii, wall thicknesses and stiffnesses lead to changes in the complex distributions of pressures and flows throughout an arterial network. These three fields have primarily been studied in isolation, and yet the properties of a single vessel emerge from the interaction of these three processes. The effect of adaptation of one artery on hemodynamics, stress, and structure of all other vessels in the network makes the arterial system a complex adaptive system that is difficult to study experimentally. This dissertation addresses this unmet need by integrating hemodynamics, vessel mechanics, and vascular adaptation by developing a novel framework with mathematical models at different scales. Allowing arteries simultaneously to adapt to mechanical stresses in a computational model of the human systemic arterial system, the present work illustrated that simple arterial adaptation to wall circumferential and endothelial shear stresses are sufficient to explain nine salient features of the cardiovascular system when traversing away from the aortic root towards the peripheral

arteries: decrease in lumen radii, wall thicknesses, vessel compliances, shear stresses, wall stresses and pulsatile flows, and increase in wall stiffnesses, pulse wave velocities, and pulsatile pressures. In addition, it revealed that pulse pressure homeostasis emerges to mechanical perturbations such as reduced ejection fraction, increased peripheral resistance and aortic coarctation. Finally, it illustrated how changes in sensitivity of arterial adaptation to pulsatile wall stress can lead to manifestations of disease states such as increased pulse wave velocity and isolated systolic hypertension. The governing principles leading to the emergence of complex, adaptive behavior in the systemic arterial system have thus been identified.

*Kính tặng mẹ, người đã luôn âm thầm dành cho con tình thương vô điều kiện để vượt qua những khó khăn, thử thách của cuộc đời.*

## ACKNOWLEDGEMENTS

I am eternally indebted to Dr. Christopher M. Quick, whose vision has helped me discover a lifelong passion in research, whose tutelage has guided me through failures, whose patience has given me adequate time to learn what is important.

There are things one learns from a prolonged graduate study that shapes one's worldview, and I wish to thank Dr. Randolph Stewart and Dr. Glen Laine, whose kindness I will always remember. I would like to thank Dr. John Criscione for inspirations and timely, succinct advices that helped steered my education. I would also like to thank all undergraduate students who have worked with me, and have taught me more than I could teach them.

It was not my determination that sustained me during this long journey, but the continual encouragements from those beside me, and towards this end I would like to thank my dearest friends: Tan Lao, Ruoming Bi, Trung Le, Dr. Bharati Hegde, Dr. Ranjeet Dongaonkar, Dr. M. Waqar Mohiuddin, Sonia E. Kinra, Sarah F. Knezek-Coquis. Your true friendships have fostered in me an appreciation for this beautiful, diverse world.

Finally, I wish to express my deepest gratitude to my family, who patiently waited for me with love and support through the trying years, and will continue to be a source of inspirations, purpose, and meaning.

## NOMENCLATURE

| | |
|---|---|
| $Q$ | Axial volumetric flow rate |
| $Q_p$ | Pulse flow, defined to be the difference between the maximum and minimum value of $Q$ for a cardiac cycle |
| $P$ | Time-dependent transmural pressure |
| $\bar{P}$ | Mean pressure, averaged over cardiac cycle |
| $\tilde{P}$ | Pulse pressure, defined to be the difference between systolic pressure and diastolic pressure for a cardiac cycle |
| $\tilde{P}_W$ | Pulse pressure of a Windkessel |
| $R'$ | Vessel resistance per unit length |
| $L'$ | Vessel inertance per unit length |
| $C'$ | Vessel compliance per unit length |
| $C$ | Total vessel compliance |
| $C_T$ | Total arterial compliance |
| $R_S$ | Total systemic vascular resistance |
| $z$ | Axial position along a vessel |
| $\omega$ | Angular frequency |
| $\lambda$ | Pulse wavelength |
| $j$ | $\sqrt{-1}$ |
| $t$ | Time |
| $\mu$ | Dynamic viscosity of blood |
| $\rho$ | Mass density of blood |

| | |
|---|---|
| $Z_o$ | Characteristic impedance |
| $Z_{in}$ | Input impedance |
| $Z_L$ | Longitudinal impedance |
| $c_o$ | Pulse wave velocity |
| $c_{ph}$ | Phase velocities |
| $\Gamma$ | Local reflection coefficient |
| $\sigma$ | Time-dependent stress acting on the arterial wall in the circumferential direction associated with a transmural pressure, averaged over wall thickness |
| $\tilde{\sigma}$ | Pulse wall stress, defined to be the difference between the maximum and minimum value of wall circumferential stress for a cardiac cycle |
| $\tau$ | Time-dependent shear stress acting on the vessel wall in the axial direction associated with an oscillating pressure gradient |
| $\sigma_{rms}$ | Square root of the mean value squared of $\sigma$ over a cardiac cycle |
| $\tau_{rms}$ | Square root of the mean value squared of $\tau$ over a cardiac cycle |
| $r$ | Vessel lumen radius |
| $h$ | Vessel wall thickness |
| $l$ | Vessel length |
| $E$ | Elastic modulus of the vessel wall, defined to be the slope of the linear approximation of the circumferential stress to the circumferential strain. |
| $r_o$ | Parameter of adaptive rule for radius, defined to be the intercept at zero stress. |
| $\alpha$ | Slope of the adaptive rule for radius, represents the sensitivity of radius adaptation to stress. |

| | |
|---|---|
| $h_o$ | Parameter of adaptive rule for wall thickness, defined to be the intercept at zero stress. |
| $\beta$ | Slope of the adaptive rule for wall thickness, represents the sensitivity of wall thickness adaptation to stress. |
| $E_o$ | Parameter of adaptive rule for elastic modulus, defined to be the intercept at zero stress. |
| $\gamma$ | Slope of the adaptive rule for elastic modulus, represents the sensitivity of stiffness adaptation to stress. |

**TABLE OF CONTENTS**

Page

## LIST OF FIGURES

# CHAPTER I

# INTRODUCTION

## Salient Features of the Mammalian Arterial System

Mammalian arterial mechanical properties, hemodynamic variables, and vascular stresses exhibit consistent trends with increasing distance from the aortic root towards the peripheral arteries. Attending a decrease in vessel lumen radius are a decrease in wall thickness and an increase in wall stiffness (52). These changes in mechanical properties correspond with a decrease in vessel compliance and increase in pulse wave velocity. As expected in a ramifying arterial tree, mean and pulsatile blood flow decrease with each branch encountered. In contrast, attending an expected small decrease in mean transmural pressure is a less intuitive *increase* in pulse pressure (systolic – diastolic pressures) toward the periphery (80). Although less often reported, circumferential wall stress and endothelial shear stress tend to decrease (3, 4). Reported explanations of the origin of these trends have necessarily been incomplete, because they have either relied on teleological arguments (34, 106, 110), or have focused on a subset of complexities by assuming heterogeneous arterial structures (63, 82, 93, 107, 111), hemodynamic properties (34, 57, 106, 110), or mechanical stresses a priori (19, 35, 49, 73, 77, 100, 101). It is generally agreed, however, that the interactions among network hemodynamics, local stresses, and vascular adaptation give rise to the observed complexities of the mammalian arterial system (28, 71).

**Chronic Regulations of Mean and Pulse Pressure by the Vasculature**

It is widely accepted that cardiac output, peripheral resistances, and vascular compliances are the primary determinants of arterial pulsatile pressures (52, 59). Whereas cardiac output and peripheral resistances are the predominant mechanical factors that determine mean pressure, compliance of the conductance arteries predominantly is the primary mechanical factor affecting pulse pressure. Mean and pulse pressure are inherently coupled. When mean pressure rises acutely, compliant arteries undergo stretch-induced stiffening of the arterial wall, [i.e., "pressure-dependent compliance" (46)], and pulse pressures rises. However, mean and pulse pressures are regulated independently of one another chronically. A sustained increase in mean arterial pressure is correlated with a gradual increase in compliance, a process commonly described as "compliance resetting" (16). The initial changes in pulse pressure due to abrupt changes in peripheral resistance and cardiac output thus may tend to ameliorate with time. Abrupt increases in pulse pressure immediately after aortic coarctation also become less pronounced with chronic adaptation (102). In each case, pulse pressure appears to be regulated independently of the regulation of mean pressure by modulation of a key mechanical property: conductance artery compliance. While aortic pulse pressure appears to be homeostatic, no mechanism yet has been identified to control pulse pressure by adaptation of local compliance.

**Quantifying Pressure Pulse Propagation and Reflection in Arterial Networks**

Arterial pressures generally do not rise and fall simultaneously throughout the systemic arterial system in young, healthy individuals (52, 59, 61). As the ventricle ejects a bolus of blood into the arterial system, a pressure pulse propagates toward the periphery and is reflected back from multiple locations (52, 59, 61). In fact, pressure pulse waves are reflected (and re-reflected) wherever a change in the impedance to blood flow is encountered, particularly at bifurcations as well as sites with local changes in geometry or stiffness (7). To capture the complex hemodynamics arising from pulse wave propagation and reflection, investigators have developed realistic, large-scale arterial system models (60, 63, 93, 107). Extending the early work of Noordergraaf (62), Westerhof et al. (107) developed a realistic human systemic arterial system model consisting of 121 arterial segments, each with different length, lumen radius, wall thickness and material stiffness (61). To calculate blood pressures and flows in each segment, they used the "transmission line equations" that incorporate the principles of conservation of mass and linear momentum (61). The classical Westerhof model formed the basis of a number of subsequent models, because it defined a standard network architecture, and collated mechanical parameters from many sources. Investigators have since refined it by adding vessels (107), adjusting parameters (93), or using more sophisticated fluid dynamic equations (82, 111). The classical Westerhof model nonetheless captures the complex transmission and reflection of pressure and flow pulses throughout the systemic arterial system (81, 93). Such models not only have reproduced the observed increase in pulse pressure toward the periphery (63, 83, 93, 107), but also the changes in pulse pressure with

increased peripheral resistance (54), decreased compliance (93), and aortic coarctation (93). The latter, in particular, has revealed that pulse pressure is highly sensitive to an abrupt local change of arterial geometry and stiffness (93). These modeling efforts have established that regional pressures and flows arise from complex interaction among vessels in a network—any change in the mechanical properties of one artery significantly affect the pulsatile pressure and flows in all other arteries.

**Degeneration of the Arterial System into a Windkessel**

It is recognized that elderly subjects tend to exhibit increased pulse pressures, decreased arterial compliances, and increased pulse wave velocities (52, 59). Given the negative impact of isolated systolic hypertension on clinical outcomes (32), the cause of increased systolic pressure has been vigorously studied, and multiple explanations have been proposed. One group of investigators, focusing on the ability of the cardiovascular system to store blood, have used the classical Windkessel model to argue that decreased total arterial compliance is the primary cause (6, 53). In this framework, when the heart ejects a volume, an inability to expand leads to a higher pulse pressure. Another group of investigators, focusing on the ability of the cardiovascular system to transmit pressure pulses, have used the sophisticated transmission models to argue that increased pulse wave velocity, due to decreased vessel compliances, is the primary cause (59). In this framework, when the heart ejects a volume, the reflected waves return to the aorta earlier in the cardiac cycle at increased velocity, and add to the antegrade waves, thus increasing pulse pressure. The second interpretation was dominant until a series of reports illustrated that reflected pulse waves do not necessarily increase pulse pressure (75), that increasing

pulse wave velocity does not necessarily cause the composite reflected wave to arrive earlier in systole (53), and that finally, an increase in pulse wave velocity (absent a decrease in arterial compliance) does not in itself raise pulse pressure (53). The fundamental insight guiding the current interpretation is that the systemic arterial system degenerates into a classical (two-element) Windkessel at high pulse wave velocities (53, 74). The physical principles underlying this observation were elucidated by Mohiuddin et al. (53) using the insight that as pulse wave velocity increases, pulse wavelength increases, and the effects of arterial network mechanical heterogeneity, branching, and topological asymmetry becomes insignificant. Pressures rise and fall almost simultaneously throughout the cardiac cycle. In fact, Mohiuddin et al. (53) illustrated that the normal stiffness of the Westerhof model, even when compliance was increased by 50% to become more consistent with later measurements (93), produced pressures with 0.95 correlation with the pressures predicted from a Windkessel.

**Loss of Arterial Compliance due to Increased Pulse Pressure**

Isolated systolic hypertension is associated with increased peripheral resistance and decreased systemic arterial compliance (6, 59). While increased peripheral resistance is often attributed to endothelial dysfunction (59), decreased arterial compliance has often been attributed to fatigue-induced stiffening (59). This traditional viewpoint attributes changes in arterial mechanical properties with age to a passive, gradual degradation of the elastic components of the arterial wall exposed to cyclical stresses (59). However, experimental evidence suggest that arteries continue to actively adapt in hypertension with smooth muscle cell hypertrophy (59) and re-arrangement structural constituents (30, 59).

Furthermore, changes in arterial mechanical properties arising from adaptive responses are relatively rapid, with changes in protein expression occurring within days (28) and complete structural remodeling within weeks (28). Indeed, arteries have been shown to exhibit a remarkable ability to adapt within weeks in human patients with end-stage renal failure (22), as well as patients who require coronary bypass surgeries (103) at advanced age. Thus, while the ability of arteries to adapt to mechanical changes may vary with age, it is retained throughout the adult life (39). Although several investigators have recently developed mathematical models incorporating more physiological explanations stiffening of arteries with age, they have in common an assumption that greater cyclical wall stress leads to a gradual loss of compliance (19, 35, 100, 101).

**Vascular Adaptation to Mechanical Stresses**

Primary and secondary hypertension has often been correlated with media-intimal thickening and stiffening of elastic arteries in both the young and elderly (17, 18, 59). Similarly, chronic increases in luminal flow with downstream metabolite-induced vasodilation and exercise has been correlated with increasing vessel lumen radius (55, 69, 86). Most mechanistic studies of adaptive behavior, however, have employed acute experiments on muscular arteries *in vitro*. Such studies have revealed that vessels are particularly sensitive to mechanical stresses, particularly endothelial shear stress and circumferential wall stress (13, 28, 85). Perturbations in luminal pressures and flows act to constrict and dilate vessels, which has been hypothesized to minimize the initial perturbation from the "homeostatic" stress values (13, 28). The insight that mechanical stresses are fundamental adaptive stimuli has been difficult to translate into the study of

chronic growth and remodeling of large elastic arteries, because of inherent difficulties culturing arteries *in vitro* (23). Furthermore, it is exceedingly difficult to control endothelial shear stress and circumferential wall stress *in vivo*. Adaptation in radius, wall thickness or stiffness affect vascular stresses, even when luminal pressure and flow are maintained (24). Furthermore, such adaptations *in vivo* can alter luminal pressures and flows (49, 70-73, 77, 78). Inability to control wall circumferential and shear as independent variables is an inescapable consequence of arterial structural remodeling *in vivo* (25).

**Inferring Adaptive Rules from Experimental Studies**

Investigators have long reported that chronic changes in blood pressure and flow *in vivo* are associated with adaptive responses that alter the mechanical properties of vessels (84, 113). Modern mechanobiology has revealed that it is not pressure and flow that directly stimulate adaptive responses in elastic arteries, but rather the mechanical stresses acting on the arterial wall (28, 85). Most mechanobiology studies, however, are performed on cultured cells to control mechanical stresses (13, 28). The inability to rigorously control stresses *in vivo* arises from a complex interaction among arterial mechanical properties, hemodynamic variables, and vascular stresses. Changes in stresses affect mechanical properties, changes in mechanical properties in turn affect hemodynamics, and changes in hemodynamics in turn affect vascular stresses. Despite the difficulty in ascribing causality from correlation of one particular vascular stress and one particular mechanical property, investigators believe that endothelial shear stress is the

predominant determinant of vessel radius (28), and circumferential wall stress is the predominant determinant of wall thickness and material stiffness (20, 52).

**Experimentally Relating Arterial Adaptation to High Pulse Pressure**

Although pulse pressure and pulse wave velocity are easily measured and correlated with clinical outcomes (45), both are very sensitive to arterial compliance. The adaptive responses that affect arterial compliance, however, are difficult to characterize experimentally. Vessel compliance depends not only on material stiffness of the arterial wall, but also wall thickness and radius (61), each of which may adapt after an intervention that affects pressures and flows, and thus the stresses sensed by mechanocytes *in vivo* (13, 28). Nonetheless, both steady and cyclic stresses have been reported to be powerful stimuli for vascular growth and remodeling (13, 28), and there is a growing body of evidence that cyclic stress or stretch impact normal cellular functions (13). Changes in cyclical stresses, in particular, have been shown to induce changes in interstitial matrix proteins, smooth muscle cell size, and stiffness of arteries (13, 28). Most mechanobiology studies, however, are performed on isolated cells, due to the difficulty of chronically culturing intact arteries *in vitro* (23). Unlike *in vitro* experiment that can precisely control imposed stresses, *in vivo* experiments suffer from the complexities arising from the interaction of hemodynamics, where arterial compliance effects pulse pressure, and adaptive processes, where pulse pressure effects arterial compliance. The fact that pulse pressure is both a cause and effect of arterial compliance has led investigators to increasingly rely on mathematical models (53, 83, 93, 107).

## Structural Adaptation of Arterial Networks

Given the difficulty in experimentally establishing causal relationships between changes in a particular mechanical property to a particular stress *in vivo*, investigators have relied heavily on mathematical modeling to characterize the structural adaptation of single vessels (19, 35, 100, 101) or entire vascular networks (73, 78). Kamiya et al. (33) suggested that adaptation of radii to mean endothelial shear stress provided a mechanistic basis of Murray's Law, a teleological argument predicting optimal geometry of an arterial bifurcation (57). Adaptation to mean endothelial shear stress subsequently was invoked in mathematical models as a critical mechanism explaining the complex distribution of radii in entire networks of microvessels (73) and conductance vessels (78). Adaptation of wall thickness to mean circumferential wall stress was also invoked in a microvascular model as a critical mechanism explaining the complex distribution of wall thicknesses (70). Such network models have not only confirmed the critical role played by endothelial shear stress and circumferential wall stress, they yielded the critical insight that a complex architecture can emerge from the *identical* adaptive rules universally applied to each vessel. The only reported mathematical model of a network of elastic vessels that incorporated pulsatile hemodynamics, however, assumed an equilibrium set point shear stress *a priori* (49).

## Simultaneous Prediction of Mechanical Properties, Hemodynamics, and Stresses in an Arterial Network

Motivated by the observation that adaptation reduces the initial perturbation in stresses *in vivo* (28), mathematical models purporting to explain the structural adaptation of vascular networks assumed vascular adaptation to mechanical stress "set points" (19,

35, 49, 100, 101). Cecchini et al. (11), however, questioned whether the set point is a distinct structural entity in biological control. Their seminal work illustrated that the set point concept, borrowed from engineered systems, is unnecessary to explain control of physiological systems. Instead, homeostasis can be achieved when a system with competing processes, providing negative feedback that yields an equilibrium "balance point". For instance, Guyton's classic cardiac output-venous return balance point made the search for a "cardiac output set point" unnecessary (11, 26). Although not explicitly invoking balance points, Liao and Kuo (44) illustrated it is possible to predict equilibrium shear stresses and radii of a simple microvascular network without assuming equilibrium set points.

# CHAPTER II

# DISSERTATION FOCUS

Arterial pulse pressure, pulse wave velocity and arterial compliance have been used as clinical indices of cardiovascular health. While sharing a common goal of relating disease states to arterial function, hemodynamicists have traditionally focused on predicting changes in pressures from assumed mechanical properties, biomechanicists on measuring changes in mechanical properties in disease states, and mechanobiologists on delineating changes in vessel adaptation to stresses. The inherent segregation in these disciplines arose from three identifiable barriers to integration: 1) A lack of an appropriate theoretical framework to characterize the dynamic equilibrium among global pulsatile hemodynamics variables, local mechanical stresses on arteries, and local stress-induced adaptation of arteries. 2) A lack of a direct method to predict simultaneous changes in arterial pulse pressure, arterial mechanical properties, and stresses as the arterial system adapts to changing mechanical demands. 3) A lack of a direct method to predict complex changes in global hemodynamics from changes in mechanotransduction of arteries. Hence, the fundamental goal of attributing global hemodynamics of interest to clinical investigators to changes in local arterial function studied by basic scientists, has remained unfulfilled. Therefore, the purpose of this dissertation is to integrate biomechanics, hemodynamics, and vascular adaptation in a multi-scale model to relate the mechanisms of vascular adaptation to arterial pulsatile pressure in health and disease. This goal will be achieved by pursuing three specific aims:

1. Use a balance point approach to identify the simplest set of universal adaptation rules that simultaneously predict observed mechanical properties, pulsatile hemodynamics, and vascular stresses throughout the human systemic arterial system.
2. Use a realistic human systemic arterial system model to test the hypothesis that global pulse pressure homeostasis can emerge from local adaptation of arteries to mechanical stresses.
3. Use an adaptive model of the arterial system to test the hypothesis that diminished ability to adapt to pulsatile wall stress can cause arterial compliance to decrease and pulse pressure to increase, leading to isolated systolic hypertension.

Achievement of these goals provides a fundamental framework to explain the emergence of arterial system complexities from simple underlying physical and biological processes, predict normal arterial system adaptation to external mechanical perturbations, and relate changes in mechanotransduction to isolated systolic hypertension, characterized by high systolic pressures, loss of arterial compliance, and increased aortic pulse wave velocity. Chapter III outlines the fundamental theory and assumptions common to all specific aims. Specific aims 1, 2, and 3 will be addressed in Chapter IV, V, and VI, respectively. Chapter VII concludes this dissertation with principles general to all three specific aims.

# CHAPTER III

# THEORY

## Pulsatile Pressure-Flow Relations in an Artery

The relationship between blood pressure and flow was characterized using a standard one-dimensional (1D), "transmission line" approach typically used for characterizing pulsatile hemodynamics in large arterial networks. With negligible body force effects, the Navier-Stokes equation, describing Newton's second law of motion in differential form, relates the velocity vector $\boldsymbol{v}$ to the pressure field $P$ for an incompressible fluid with a dynamic viscosity $\mu$ and density $\rho$.

$$\rho \frac{D\boldsymbol{v}}{Dt} = \nabla P + \mu \nabla^2 \boldsymbol{v} \tag{1a}$$

Neglecting irrotational and radial flow, as well as entrance effects, the Navier-Stokes equation may be written in terms of the vessel's axial position z.

$$\rho \frac{\partial v_z}{\partial t} = -\frac{\partial P}{\partial t} + \mu \left[\frac{1}{r}\frac{\partial}{\partial \hat{r}}\left(\hat{r}\frac{\partial v_z}{\partial \hat{r}}\right)\right] \tag{1b}$$

The velocity profile $v_z$ can thus be solved explicitly in terms of the time t and radial position $\hat{r}$ (i.e., Womersley's solution). To relate pulsatile pressure and flow, however, a mathematically simpler approach can be taken by first noting that the integral of the dot product between $v_z$ across the vessel cross-sectional area is the volumetric flow rate $Q$.

$$\rho \frac{\partial}{\partial t}\int_0^r \int_0^\theta v_r r dr d\theta = -\frac{\partial P}{\partial t}\int_0^r \int_0^\theta r dr d\theta + \mu \int_0^r \int_0^\theta v_r dr d\theta \tag{1c}$$

Using a parabolic, oscillating velocity profile as an approximation, the peak velocity at the centerline ($\hat{r} = 0$) can be obtained in terms of flow rate.

$$v_z(0) = \frac{2}{\pi r} Q \tag{1d}$$

Hence, the equation of motion simplifies into a first-order, linear differential equation relating pressures and flows.

$$\frac{\rho}{\pi r^2}\frac{\partial Q}{\partial t} = -\frac{\partial P}{\partial t} + \frac{8\mu}{\pi r^4} Q \tag{1e}$$

The ratio $\rho/\pi r^4$ characterizes inertial effects, and the ratio $8\mu/\pi r^4$ characterizes viscous effects. They are typically referred to as the inertance per unit length ($R'$) and resistance per unit length ($L'$).

$$R' = \frac{8\mu}{\pi r^4} \tag{1f}$$

$$L' = \frac{\rho}{\pi r^2} \tag{1g}$$

For a compliant vessel, mass balance requires that the rate of change of flow in the axial direction must be equal to the rate of change of volume the vessel due to distension. Since mass balance is defined point-wise along the vessel, for a vessel with constant length ($l$) the change in volume is proportional to the change in cross-sectional area $S$ ($S = V/l$).

$$-\frac{\partial Q}{\partial t} = \frac{\partial S}{\partial t} \tag{2a}$$

The change in $S$ with respect to time, in turn, depends on the change in the distending pressure $P$.

$$\frac{\partial S}{\partial t} = \frac{\partial S}{\partial P}\frac{\partial P}{\partial t} \tag{2b}$$

The ratio $\partial S/\partial P$ characterizes the structural property of the vessel wall, and is often referred to as the compliance per unit length ($C'$). For a thick-walled vessel, $C'$ may be directly computed from the vessel the vessel luminal radius ($r$), wall thickness ($h$), and elastic modulus ($E$).

$$C' = \frac{3\pi r^2(r+h)^2}{Eh(2r+h)} \quad (2c)$$

The elastic modulus ($E$) of the arterial wall relates the circumferential wall strain to the circumferential wall stress, typically called the Young's modulus in the classical literature (52, 59, 61), and thus describes the material stiffness of the vessel wall. Together, the statements of linear momentum balance and mass balance form a system of differential equation relating pressure and flow to the inertance, resistance, and compliance of a vessel, which together characterize the solid-fluid interaction that governs pulse wave propagation.

$$-\frac{dP}{dz} = R' \cdot Q + L' \frac{dQ}{dt}. \quad (3a)$$

$$-\frac{dQ}{dz} = C' \frac{dP}{dt}. \quad (3b)$$

*Eqs. 3a* and *3b* may be combined to yield a single, second-order differential equation as a combined statement of linear momentum and mass balance,

$$-\frac{\partial^2 P}{\partial z^2} = L'C' \frac{\partial^2 P}{\partial t^t} + R'C' \frac{\partial P}{dt} \quad (3c)$$

*Eq. 3c* is commonly known as the "wave equation". For compliant vessels, pressure pulse wave travels at finite speeds. The wave speed $c$ is related to the second derivative of pressure with respect to both space and time, and is defined as follow.

$$\frac{\partial^2 P}{\partial z^2} = \frac{1}{c^2} \frac{\partial^2 P}{\partial t^2} \quad (3d)$$

Thus in the frequency domain, the *phase velocities ($c_{ph}$)* can be computed directly from *Eq. 3c* and *3d* in terms of the angular frequency $\omega$.

$$c_{ph} = \frac{j\omega}{\sqrt{(j\omega L' + R')j\omega C'}} \quad (3e)$$

The wave equation admits a unique, general solution in terms of $c_{ph}$.

$$P(z,\omega,t) = \left(p_f e^{-j\omega z/c_{ph}} + p_r e^{-j\omega z/c_{ph}}\right) e^{-j\omega t} \quad (3f)$$

The variables $p_f$ and $p_r$ characterizes the antegrade and reflected waves, respectively. To relate the pulsatile pressure $P$ to the pulsatile pressure $Q$, an input impedance $Z_{in}$ can be defined.

$$Z_{in}(\omega) = \frac{P(\omega)}{Q(\omega)} \quad (3g)$$

The input impedance can be written in terms of the global reflection factor $\Gamma$ and characteristic impedance of the vessel $Z_o$ (61).

$$Z_{in} = Z_o \frac{1+\Gamma}{1-\Gamma} \quad (3g)$$

The characteristic impedance is an intrinsic property of the vessel segment, also defined per unit length in terms of inertance, resistance, and compliance.

$$Z_o = \sqrt{\frac{j\omega L' + R'}{j\omega C'}} \quad (3h)$$

The reflection factor, however, depends also on the vessel length l and the input impedance of the downstream network, commonly referred to as the load impedance ($Z_L$).

$$\Gamma = \frac{Z_L - Z_o}{Z_L - Z_o} e^{2j\omega l/c_{ph}} \quad (3h)$$

Thus given the values of *r, h*, and *E* for all vessels in the network, as well as blood viscosity and density, the values of local pressures and flows for each vessel segment can be calculated using standard methods (59).

**Mechanical Stresses on Arteries**

Consistent with a one-dimensional approach to describe hemodynamics, only the spatially-averaged values of wall circumferential stress acting on the arterial wall and the shear stress acting on the endothelium were considered. The time-dependent circumferential wall stress ($\sigma$) was calculated using Laplace's law using the time-dependent pressure at the entrance of the vessel,

$$\sigma(t) = \frac{r}{h} \cdot P(t). \tag{4}$$

The endothelial shear stress ($\tau$) was calculated by assuming an oscillating parabolic velocity profile (20, 52, 82),

$$\tau(\omega) = \frac{r}{2} Z_L(\omega) \cdot Q(\omega). \tag{5a}$$

Since radius may vary in all vessels over a wide range, to speed up simulations, the ratio of inertial to viscous effects was assumed to be negligible, and *Eq*. *5a* simplifies,

$$\tau(t) = \frac{4\mu}{\pi r^3} \cdot Q(t). \tag{5b}$$

To fully capture the effects of both mean and pulsatile values of wall and shear stresses, the root of the mean squared (RMS) values of the mechanical stimuli ($\sigma_{rms}$ and $\tau_{rms}$, respectively) defined over the cardiac cycle *T* were used.

$$\sigma_{rms} = \sqrt{\frac{1}{T}\int_0^T \sigma(t)^2 \, dt} \tag{6}$$

$$\tau_{rms} = \sqrt{\frac{1}{T}\int_0^T \tau(t)^2 \, dt} \tag{7}$$

The values of these "effective" stresses reflect contributions of both the steady and pulsatile components of circumferential wall stress and endothelial shear stress.

**Hemodynamic Coupling of Mechanical Stresses**

Circumferential wall stress and endothelial shear stress are highly coupled. In a straight, cylindrical segment of artery, $\sigma$ and $\tau$ at any axial position $z$ can be computed directly from the transmural pressure $P$ and the pressure gradient $dP/dz$ (29).

$$\sigma = \frac{r}{h}P \tag{8}$$

$$\tau = \frac{r}{2}\frac{dP}{dz} \tag{9}$$

When the cardiovascular system behaves as a linear, time-invariant system, the equations relating flow and pressures are linear in the frequency domain (52, 61), and the relationship between pulsatile transmural pressure to pulsatile axial flow ($Q$) is characterized by the frequency-dependent the input impedance ($Z_{in}$).

$$Z_{in}(\omega) = \frac{P(\omega)}{Q(\omega)} \tag{10}$$

While is the ratio of the transmural pressure to axial flow is the input impedance, the ratio of the oscillating pressure gradient to the axial flow is the longitudinal impedance ($Z_L$).

$$Z_L(\omega) = \frac{dP(\omega)}{dz}/Q(\omega) \tag{11}$$

In addition, $Z_L$ can be expressed in terms of the frequency-dependent phase velocity ($c_{ph}$) and vessel characteristic impedance ($Z_o$) (61).

$$Z_L = j\omega\frac{Z_o}{c_{ph}} \tag{12}$$

The wavelength ($\lambda$) of a pulse wave defined to be the ratio between $\omega$ to $c_{ph}$.

$$\lambda = \frac{\omega}{c_{ph}} \tag{13}$$

Thus the ratio of wall stress to shear stress can be found in terms of hemodynamic and structural variables from solving *Eqs. 8-13*.

$$\frac{\sigma}{\tau} = \frac{2l}{h}\frac{Z_{in}}{jZ_o}\frac{\lambda}{l} \tag{14}$$

The ratio of wall circumferential stress and shear stress therefore is a complex function with a magnitude and phase, as expected (i.e., wall stress and shear stress are out of phase *in vivo*). The magnitude of $\sigma/\tau$ thus can be expressed in terms of three hemodynamic and structural ratios.

$$\left|\frac{\sigma}{\tau}\right| = \frac{2l}{h}\frac{\lambda}{l}\left|\frac{Z_{in}}{Z_o}\right| \tag{15}$$

The ratios $l/h$, $\lambda/l$, and $|Z_{in}/Z_o|$ are known invariants in the aortas of mammals (14, 15, 87, 89, 105, 108, 109). Hence, $|\sigma/\tau|$ is invariant across mammalian species. Perhaps more importantly for the present work, *Eq. 15* demonstrates from accepted principles that wall circumferential stress and shear stress are tightly coupled in the aorta of a particular arterial system.

# CHAPTER IV

# EMERGENCE OF ARTERIAL COMPLEXITIES

## Problem Statement

Arterial mechanical properties, pulsatile hemodynamic variables and mechanical vascular stresses vary significantly throughout the systemic arterial system. Although there is a consensus on a standard set of physical laws to predict hemodynamics in a network, extant hemodynamic models all assume complex, heterogeneous distribution of mechanical properties *a priori*. Previously reported mathematical models have suggested mechanical properties adapt to achieve assumed target stress "set points". Simultaneous prediction of the mechanical properties, hemodynamics, and stresses, however, requires that neither equilibrium mechanical properties nor stresses can be assumed *a priori*. Therefore, the purpose of this chapter is to use a "balance point" approach to identify the simplest set of universal adaptation rules that simultaneously predict observed mechanical properties, hemodynamics and stresses throughout the human systemic arterial system.

## Methods

*Assumed Vascular Network Structure*. The classical Westerhof model (107), which applies *Eqs. 1-3* to a distributed human systemic arterial network consisting of 121 arterial segments (Fig. 1) was extended to incorporate arterial adaptation. The details of the model are described elsewhere (107), as well as validation in later implementations (82, 93). The original values for vessel lengths and terminal resistances reported by Westerhof et al. (107) were employed for the present work.

*Assumed Input Aortic Flow.* To simplify, an input blood flow from the heart into the aortic root was assumed. The inlet pulsatile flow was reproduced from the waveform reported by Stergiopulos et al. (92) (Fig. 12A, solid line). The magnitude and period were adjusted to produce a systolic pressure of 120 mmHg and a diastolic pressure of 80 mmHg in the ascending aorta of the classical Westerhof model (107), with compliances increased by 50% (92) at a heart rate of 72 beats per minute.

*Modeling Adaptive Responses of Arteries to Mechanical Stress.* To simplify, radius ($r$), wall thickness ($h$) and elastic modulus ($E$) was assumed to adapt independently of each other in response to vascular stresses. Specifically, radius adapts to shear stress while wall thickness and elastic modulus adapt to wall stress. These rules were based on consensus for the most commonly assumed stimulus for each mechanical property (19, 35, 71, 73, 77, 100, 101). Two principles further constrained our formulation of the adaptive rules. First, a complex, nonlinear function may be approximated by a linear one. Second, adaptive processes must provide negative feedback to ensure stability. Taken together, these assumptions lead to three simple linear equations

$$r = r_o + \alpha \cdot \tau_{rms}, \tag{16a}$$

$$h = h_o + \beta \cdot \sigma_{rms}, \tag{16b}$$

$$E = E_o - \gamma \cdot \sigma_{rms}. \tag{16c}$$

The constant parameters characterizing adaptation ($r_o$, $\alpha$, $h_o$, $\beta$, $E_o$, and $\gamma$) were assumed equal for all 121 vessel segments in the arterial network. To examine the possibility that similar equilibria can arise from assuming alternative adaptive rules, an alternative set of

adaptive rules were prescribed, letting radius adapts to circumferential wall stress while wall thickness and elastic modulus adapt to endothelial shear stress. Thus in an alternative simulation, three different linear adaptive rules were prescribed following the same principles guiding the consensus adaptive rules (*Eq. 17*).

$$r = \hat{r}_o - \hat{\alpha} \cdot \sigma_{rms} \tag{17a}$$

$$h = \hat{h}_o - \hat{\beta} \cdot \tau_{rms} \tag{17b}$$

$$E = \hat{E}_o + \hat{\gamma} \cdot \tau_{rms} \tag{17c}$$

The parameters $\hat{r}_o$, $\hat{\alpha}$, $\hat{h}_o$, $\hat{\beta}$, $\hat{E}_o$, and $\hat{\gamma}$ were also assumed equal for all 121 vessel segments. Thus each vessel in the arterial network model are assigned 3 identical adaptive rules with identical parameters for the conventional simulation (*Eq. 16*) and a different set of rules for the alternative simulation (*Eq. 17*). Cardiac output, vessel lengths, and peripheral resistances are identical for the conventional and alternative simulations. Steady state criteria and simulation step size were also kept constant for both simulations.

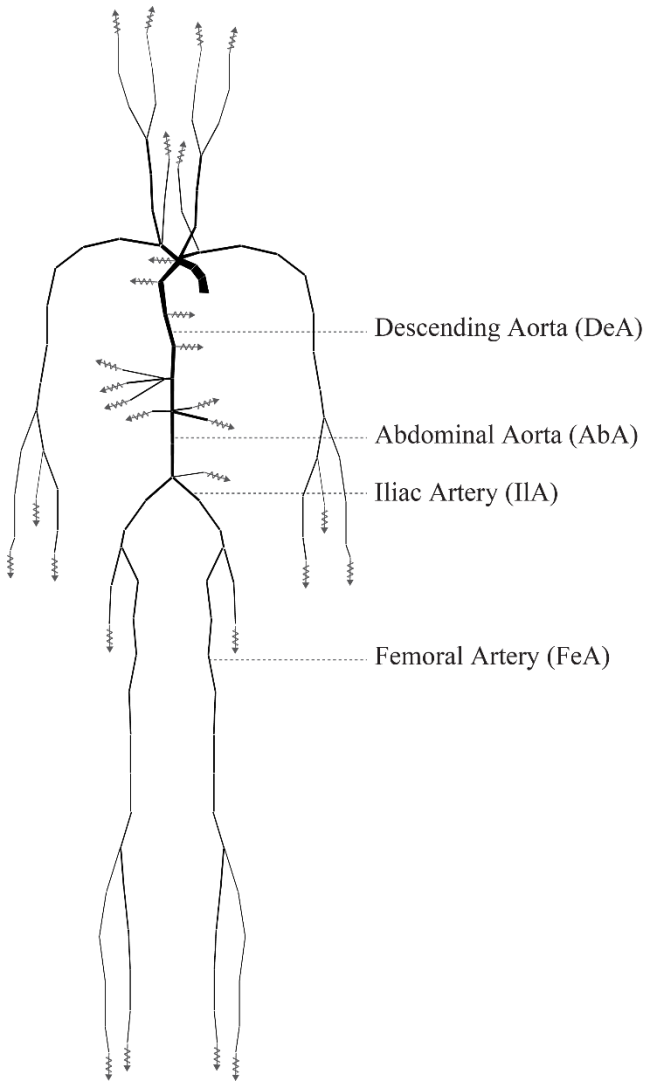


**Figure 1: Illustration of the systemic arterial network model consisting of 121 vessel segments drawn to scale according to radii and lengths reported by Westerhof et al. (107). Arteries are terminated by resistances with values also reported by Westerhof et al. (107). Flow into the aortic root modified from Stergiopulos et al. (92).**

*Iterative Method to Determine Equilibrium Variables*. *Equations 1-8* form a system of equations that can be iteratively solved for the variables $r$, $h$, $E$, $P$, $Q$, $\sigma$, $\tau$, $\sigma_{rms}$, and $\tau_{rms}$ assuming parameters characterizing adaptation ($r_o$, $\alpha$, $h_o$, $\beta$, $E_o$, and $\gamma$) have *the same* values for all vessel segments in the network. The iterative process to calculate equilibrium variables can be summarized: 1) assume initial values for $r$, $h$ and $E$ for all segments, 2) calculate values of $P(t)$ and $Q(t)$ for each segment using *Eqs. 1-3*, 3) calculate $\sigma_{rms}$, and $\tau_{rms}$ using *Eqs. 4-7*, 4) calculate new values of $r$, $h$ and $E$ from $\sigma_{rms}$ and $\tau_{rms}$ using *Eq. 16*. Steps 2-4, illustrated in Fig. 2, are iterated until steady state is reached. Steady state was assumed to be adequately achieved when the values of $r$, $h$ and $E$ were within 0.001% of the values obtained in the previous iteration. Throughout the simulation, the parameters for adaptive rules ($r_o$, $\alpha$, $h_o$, $\beta$, $E_o$, and $\gamma$) were kept constant. The initial values of $r$, $h$ and $E$ for all vessel segments were arbitrarily chosen to be 1 mm, 1 mm and 100 kPa, respectively. To verify that equilibrium is insensitive to initial conditions, two independent simulations with different initial conditions were performed: 1) randomly generated positive values of $r$, $h$, and $E$, and 2) $\sigma_{\text{rms}}$ and $\tau_{\text{rms}}$ both with values of 1 Pa. To reduce error in pressure pulse morphology, all arterial mechanical properties were allowed to adapt iteratively except the radii of the ascending aorta, which were kept constant at values originally reported by Westerhof et al. (107).

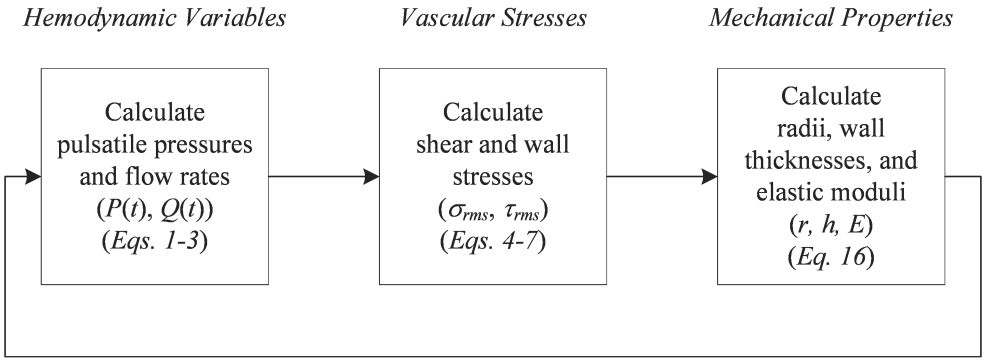


**Figure 2: Iterative process to calculate equilibrium hemodynamic variables, vascular stresses and structural properties. From initial values for radius (*r*), wall thickness (*h*), and elastic modulus (*E*), the values of pressures (*P*) and flows (*Q*) were calculated for each of 121 vessel segments illustrated in Fig. 1. From pressures and flows, mechanical stresses ($\sigma_{rms}$, $\tau_{rms}$) were calculated for each vessel. Finally, new values for *r*, *h*, and *E* were calculated using adaptive rules. The process is repeated until steady state is achieved.**

*Parameter Estimation Procedure to Estimate Values of Adaptive Parameters*. To simultaneously predict mechanical properties, hemodynamic variables, and stresses, the parameters characterizing the adaptive process $r_o$, $\alpha$, $h_o$, $\beta$, $E_o$, and $\gamma$ must be prescribed *a priori*. Without the ability to rigorously control vascular stresses *in vivo*, these parameter values cannot be directly measured, but instead must be inferred from data reported in the literature. The original values of *r*, *h* and *E* reported by Westerhof et al (107) were used, with one major caveat. Because Stergiopolis et al. (93) illustrated that the vascular compliance of the original Westerhof model were approximately 50% too low (93), the values of *E* for the current work were assumed to be 50% lower than those reported by Westerhof et al. (107). Parameter values were then estimated by linear regression from the relationships between *r*, *h*, and *E/1.5* and computed values of $\sigma_{rms}$ and $\tau_{rms}$ (107). Once it was confirmed that the inferred parameter values of $r_o$, $\alpha$, $h_o$, $\beta$, $E_o$, and $\gamma$ can yield a stable equilibria, they were fine-tuned by curve-fitting procedures to better approximate values of *r*, *h*, *E/1.5*, as well as corresponding calculated pulse pressure (systolic – diastolic) and pulse flow (peak – trough). In particular, a simple gradient descent method was used to minimize a "cost function", defined as average of the mean percentage errors in predicted *r*, *h*, *E/1.5*, pulse pressure, and pulse flow. To avoid unnecessarily weighting the impact of multiple peripheral vessels, the cost function did not include duplicate vessels (i.e., symmetrical vessels along one side of the body was not used).

*Graphical Balance Point Analysis to Characterize Equilibrium Structure and Stress*. To illustrate the interaction between mechanical properties ($r$, $h$, and $E$) and vascular stresses ($\sigma_{rms}$ and $\tau_{rms}$), standard balance point graphs were constructed that yield equilibrium values in a vessel segment of the descending aorta (Fig. 1). First, the hemodynamic (*Eqs. 1-3*) and stress equations (*Eqs. 4 - 7*) were solved $\tau_{rms}$ was graphed as $r$ was altered over a wide range. This relationship characterizes the segment's biomechanics. The structural variables of all other arterial segments were kept constant in the process. Then on the same plot equation (*Eq. 16a*) $r$ was graphed as $\tau_{rms}$ was altered over a wide range. This relationship characterizes the segment's mechanobiology. The intersection of the two graphs represents a balance point yielding equilibrium values of $r$ and $\tau_{rms}$. This process of creating a graphical balance point was repeated to characterize the interaction biomechanics and mechanobiology yielding equilibrium values of $h$ and $\sigma_{rms}$ as well as $E$ and $\sigma_{rms}$.

*Graphical Illustration of Emergent Structural Heterogeneity from Homogenous Adaptive Rules.* To illustrate the principle that a homogenous adaptive rule can yield heterogeneous mechanical properties, a standard balance point graph was constructed for four representative vessel segments along a pathway from the descending aorta to the femoral artery, illustrated in Fig. 1. In this case, the relationships between the shear stresses and radii, representing biomechanics of each vessel, were solved from *Eqs. 1-3, 5* and *7* and plotted. On the same graph, the universal adaptive rule (*Eq. 16a*) was plotted. Multiple intersections represent multiple, heterogeneous equilibria arising from the unique mechanical environment of each vessel segment.

*Pressure Morphology.* To illustrate the dynamic nature of pressure along the aorta, the transmural pressure versus time was plotted for a cardiac cycle for seven vessel segments at increasing distance for the aortic root. The distance from the aortic root was chosen for vessel segments with lengths defined by Westerhof et al. (107).

*Model Validation.* Reported average values of *in vivo* measurements of pulse pressure, pulse flow, mean endothelial shear stress, and mean circumferential wall stress were compiled for comparison with model predictions. Measured pulse wave velocities, a clinical index of arterial stiffness (59), are also compiled for model validation.

**Results**

*Numerical Values for Adaptive Parameters.* Values of parameters resulting in stable equilibria for $r$, $h$, and $E$ were identified for the conventional adaptive rules listed in *Eq. 16* (Table 1). Parameter values resulting in stable equilibria for $r$, $h$, and $E$ were identified for these alternative adaptive rules and reported in Table 2. Stable equilibria were also found for $h$, $E$, $P$, $Q$, $\tau_{rms}$ and $\sigma_{rms}$. The associated mean percentage error for $r$, $h$, and $E$ for the alternative set were similar to the mean errors arising from the consensus adaptive rules characterized by *Eq. 16*.

*Balance Point Graphs.* The resulting balance point graphs for the consensus adaptive rules (*Eq. 16*) are illustrated in Fig. 3. Stresses derived from solving hemodynamics (*Eqs. 1-3*) and stress equations (*Eqs. 4-7*) are denoted by the solid curves (i.e., biomechanics), and $r$, $h$, and $E$ derived from the adaptive rules (*Eq. 16*) are denoted by dashed lines (i.e., mechanobiology). Equilibria are indicated by the intersection of the

curves (circles). For each graph, curves have opposite slopes, indicating the presence of negative feedback.

*Graphical Illustration of Emergent Heterogeneity.* Figure 4 illustrates the balance points for radii and shear stresses for arterial segments along the aortic-femoral pathway (Fig. 1). For each vessel, there is a unique hemodynamic curve (solid line) emerging from the vessel's unique location in the network. In all vessels, however, the general behavior is similar: $\tau_{rms}$ decreases with increasing radius. For the same adaptive rule (dashed line), the equilibrium points (circles) for $r$ and $\tau_{rms}$ are unique to each vessel segment.

*Prediction of Stable Equilibria.* Simulating the simultaneous adaptation of $r$ to $\tau_{rms}$, $h$ to $\sigma_{rms}$, and $E$ to $\sigma_{rms}$ with parameters given in Table 1 resulted in stable equilibria for $h$, $E$, $P$, $Q$ and $\tau_{rms}$ and $\sigma_{rms}$. All values of $r$, $h$ and $E$ increased from the prescribed initial values of 1 mm, 1mm, and 100 kPa, respectively. Equilibria were not sensitive to initial values assumed. Alternative simulations with different initial conditions (i.e., $\sigma_{rms} = \tau_{rms} = 1$ Pa) resulted in the same equilibrium values.

| | |
|---|---|
| $r_o$ (cm) | 0.041 |
| $\alpha$ (cm$^3$/dyne) | 0.044 |
| $h_o$ (cm) | $7.5 \times 10^{-5}$ |
| $\beta$ (cm$^3$/dyne) | $1.44 \times 10^{-7}$ |
| $E_o$ (100 kPa) | 15 |
| $\gamma$ (unitless) | $1.27 \times 10^{-5}$ |

**Table 1: Numerical values of parameters characterizing the consensus rules governing adaptation of radius to shear stress ($r_o$, $\alpha$), wall thickness to circumferential wall stress ($h_o$, $\beta$), and elastic modulus to circumferential wall stress ($E_o$, $\gamma$) characterized by *Eq. 16*.**

| | |
|---|---|
| $\hat{r}_o$ (cm) | 0.87 |
| $\hat{\alpha}$ (cm$^2$/dyne) | 1.04 x $10^{-6}$ |
| $\hat{h}_o$ (cm) | 0.085 |
| $\hat{\beta}$(cm$^2$/dyne) | 1.20 x $10^{-3}$ |
| $\hat{E}_o$ ($10^6$ dyne/cm$^2$) | 3.8 |
| $\hat{\gamma}$ (unitless) | 0.096 |

**Table 2: Numerical values of parameters characterizing the alternative rules governing adaptation of radius to circumferential wall stress ($\hat{r}_o$, $\hat{\alpha}$), wall thickness to endothelial shear stress ($\hat{h}_o$, $\hat{\beta}$), and elastic modulus to endothelial shear stress ($\hat{E}_o$, $\hat{\gamma}$) characterized by *Eq. 17*.**

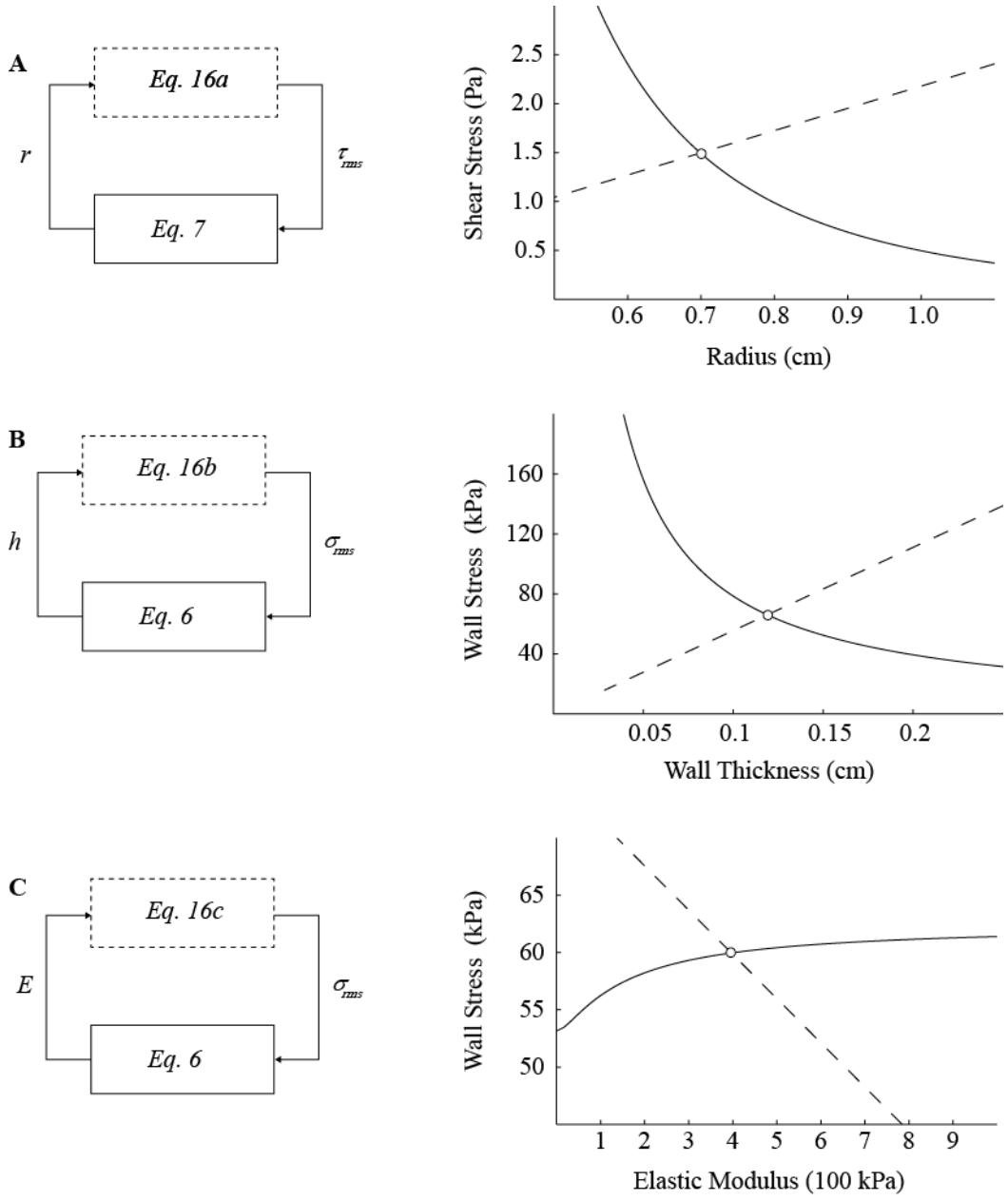


**Figure 3: Transfer functions (left) and balance point graphs (right) illustrating interaction between A) radius (*r*) and endothelial shear stress ($\tau_{rms}$), B) wall thickness (*h*) and circumferential wall stress ($\sigma_{rms}$), and C) wall material stiffness (*E*) and circumferential wall stress. The intersections (circles) between the biomechanics curves (solid curves) and adaptation lines (dashed lines) represent equilibria *r*, *h*, *E*, $\tau_{rms}$, and $\sigma_{rms}$ of this particular vessel segment.**

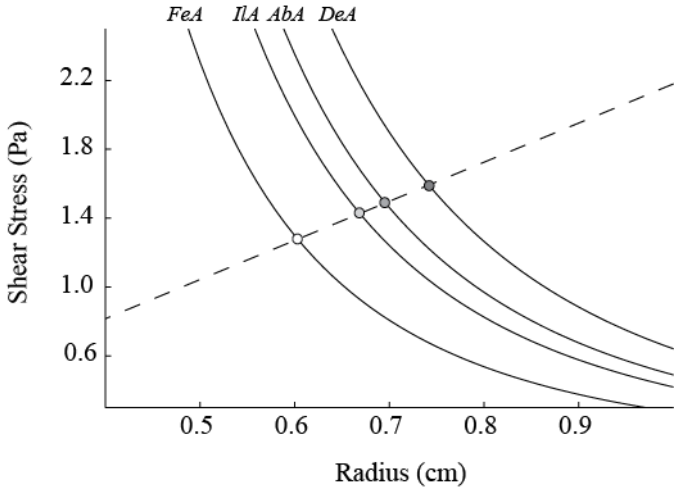


**Figure 4: Graphical illustration of the interaction between local mechanics (endothelial shear stress) and mechanical properties (vessel radius) for four representative vessel segments illustrated in Fig. 1 (DeA: descending aorta, AbA: abdominal aorta, IlA: iliac artery, FeA: femoral artery). Each hemodynamic curve (solid line) represents the segment's unique influence on its local mechanical stimuli. While all vessels were given an identical adaptive response (*Eq. 16a*, dashed line), the equilibria (circles) for radii and endothelial shear stresses are unique for each vessel.**

*Values of Equilibrium Mechanical Properties.* In equilibrium, all values for $r$, $h$, and $E$ are unique to each vessel segment. Figure 5 compares the values of $r$, $h$, and $E$ approximated by the conventional adaptive rules (solid bars) to those employed by Westerhof et al. (107) (white bars). Vessel segment numbers correspond to vessels originally reported in Westerhof et al. (107). With a few exceptions, a smaller vessel number indicates smaller distance to the aortic root (e.g., 1: ascending aorta, 2: aortic arch, 3: descending aorta).

*Trends of Equilibrium Mechanical Properties from Aorta to Femoral Artery.* To illustrate spatial trends in mechanical properties, equilibrium values of $r$, $h$, and $E$ are plotted against distance from the aortic root along the aortic-femoral pathway in Fig. 6. While both radii and wall thickness decreases with increasing distance from the aorta to the femoral artery, elastic modulus increases.

*Values and Trend of Equilibrium Hemodynamic Variables.* The equilibrium values of pulsatile pressure and flow are unique to each vessel segment. While pulse pressure gradually increases with increasing distance from the aortic root before reaching a plateau (Fig. 7A), the amplitude of flow gradually decreases with increasing distance from the aortic root (Fig. 7B). Systolic pressure increased from 113 mmHg in the descending aorta to 124 mmHg in the femoral artery, while peak flow decreased from 340 ml/s to 56.2 ml/s.

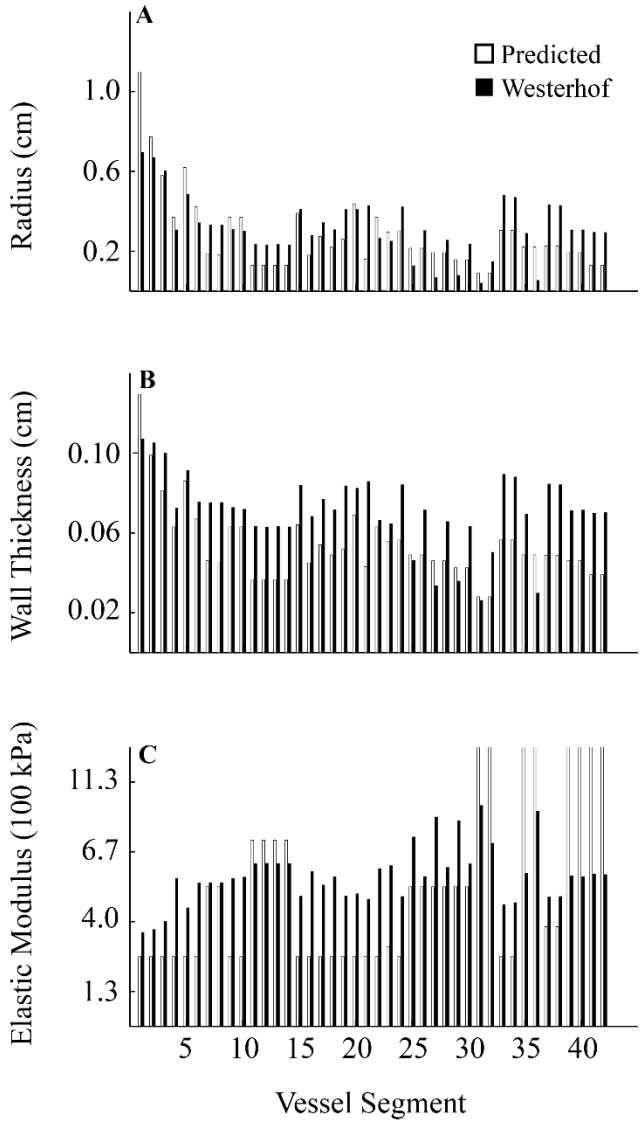


**Figure 5: Model radius, wall thickness, and elastic moduli predicted from the adaptive model compared to values reported by Westerhof et al. (107). The original values of the elastic moduli reported by Westerhof et al. (107) were divided by 1.5 to be consistent with data from Stergiopulos et al. (93).**

*Values and Trend of Equilibrium Vascular Stresses.* The equilibrium RMS values of wall circumferential stress and endothelial shear stress are also unique to each vessel segment, with both decreasing with increasing distance from the aortic root (Fig. 7C and 7D). Peak wall stress decreased from 99.4 kPa in the descending aorta to 89.2 kPa in the femoral artery, while peak shear stress decreased from 4.16 Pa to 1.95 Pa. The RMS values of wall stress and shear stress are reported in Fig. 7.

*Pressure Pulse Morphology.* At increasing distances from the aortic root, systolic pressure gradually increases while diastolic pressure slightly decreases (Fig. 8). There is a slight increase in time shift with increasing distance from the aortic root. The morphology of the pressure waveform also changes.

*Model Validation.* Predicted values of pulsatile pressures and flows and vascular stresses for various arteries are compared to *in vivo* measurements reported for young, healthy human subjects in Fig. 9. Predicted values of pulse wave velocities are compared to reported values in Fig. 10. The values of adaptive parameters (i.e., $r_o$, $\alpha$, $h_o$, $\beta$, $E_o$, and $\gamma$) yielded pulse pressures, pulse flows, wall stresses and shear stresses within reported range, while resulting pulse wave velocity is generally higher than reported values.

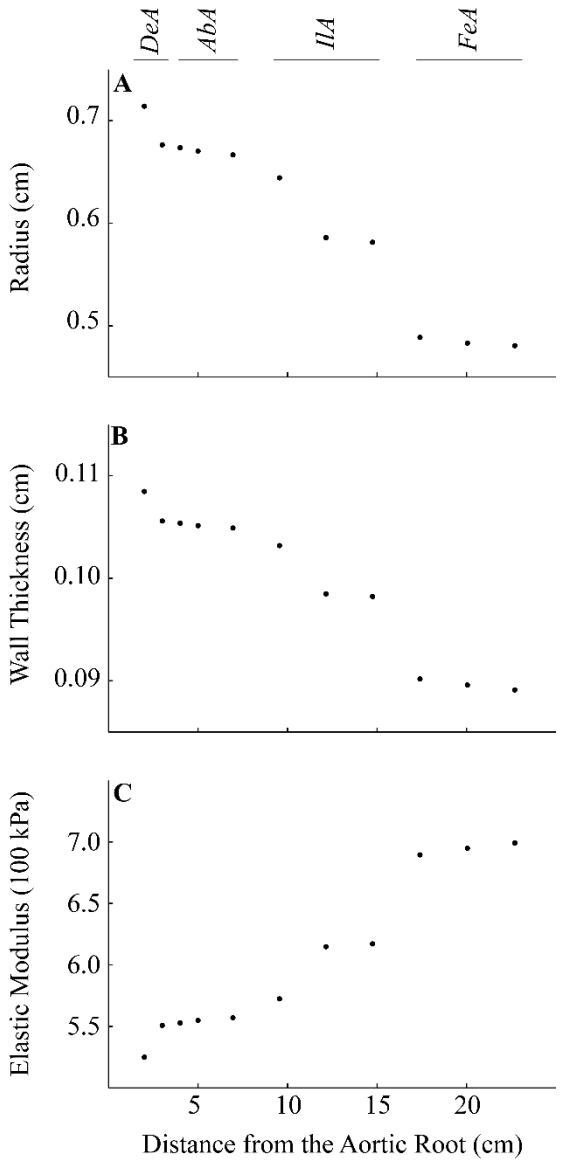


**Figure 6: Predicted values of lumen radius (A), wall thickness (B), and material stiffness characterized by tangential elastic modulus (C) for vessel segments along the aortic-femoral pathway. Consistent with reported trends (52, 59), radius and wall thickness decrease with increasing distance from the aortic root, while material stiffness increases.**

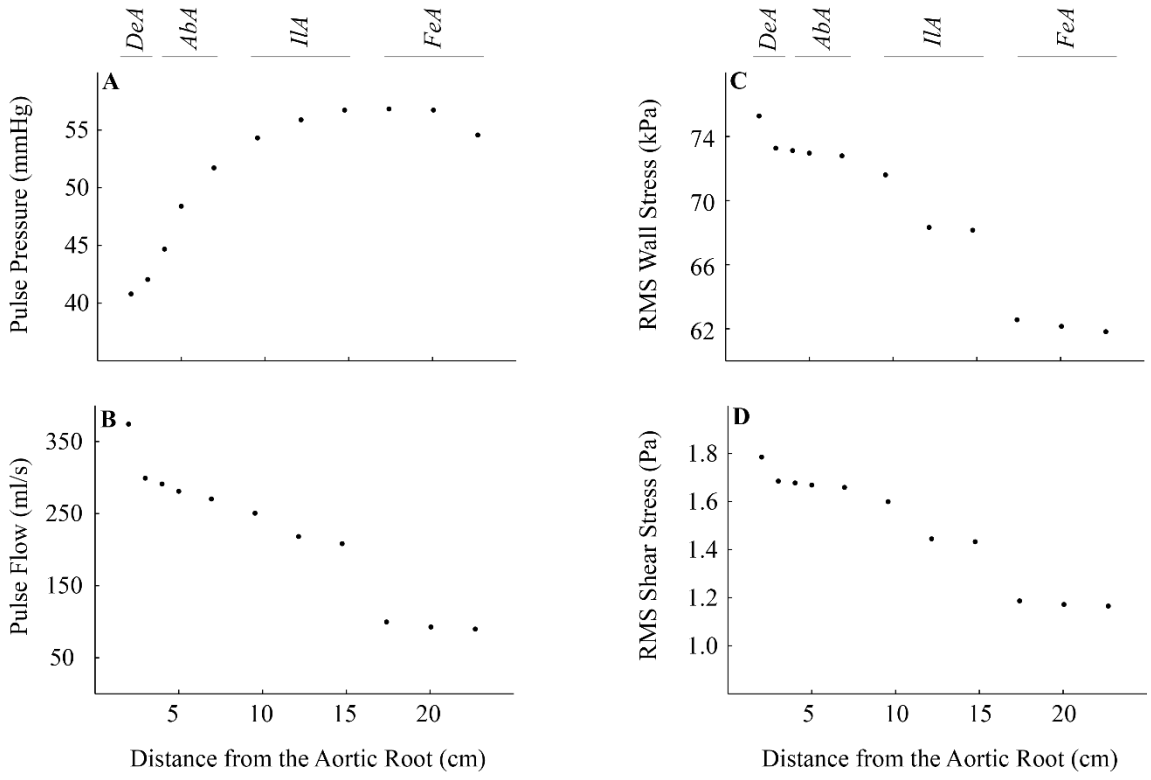


**Figure 7: Predicted trends in pulse pressure (A), pulse flow (B), RMS values of wall stress (C), and RMS values of shear stress (C). Consistent with reported trends, pulse pressure are higher in the abdominal aorta (AbA), iliac artery (IlA), and femoral artery (FeA) compared to the descending aorta (DeA), while pulse flow is lower (52, 59). The RMS values of both wall stress and shear stress are both lower with increasing distance from the aortic root.**

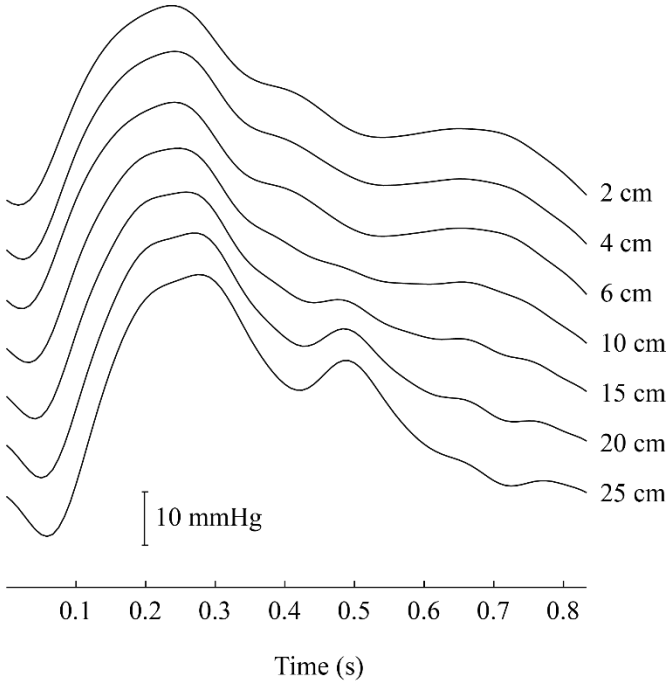


**Figure 8: Predicted time-dependent blood pressure in vessel segments along the aortic-femoral pathway illustrated in Fig. 1. Consistent with reported trends (52, 59), the systolic pressure shows a gradual increase along the aortic-femoral pathway while diastolic slightly decreases.**

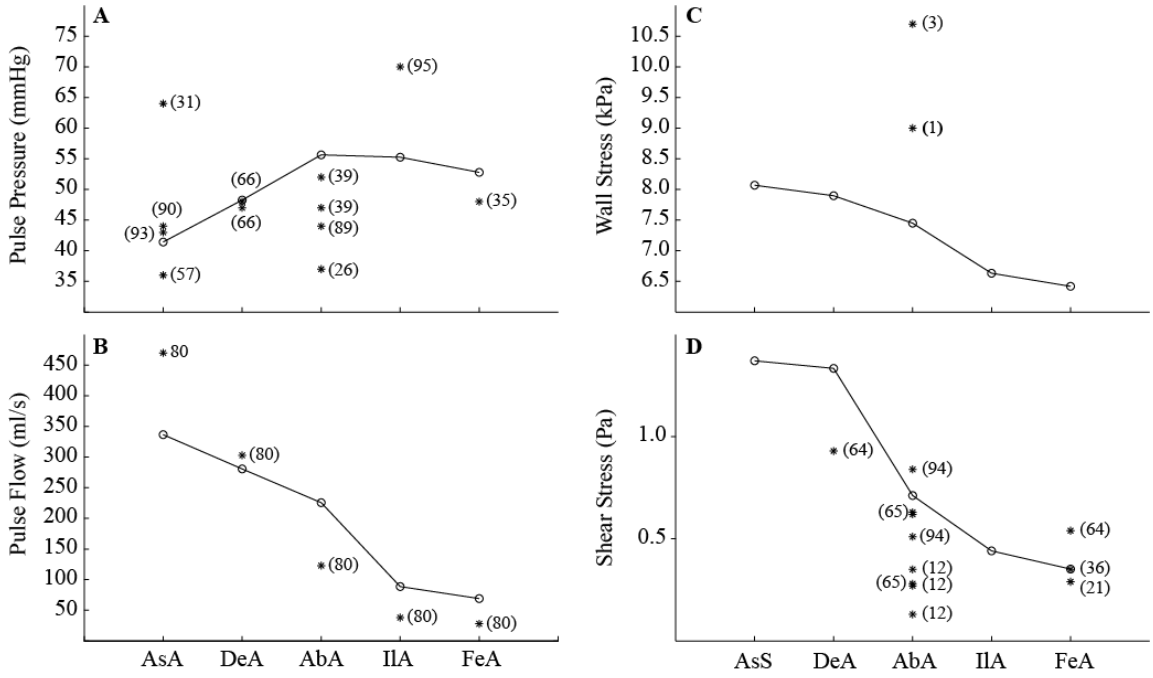


**Figure 9: Comparison between model predictions and reported values for pulse pressure (A), pulse flow (B), mean circumferential wall stress (C), and mean endothelial shear stress (D). Number next to data point denotes the relevant references: (3, 12, 21, 27, 31, 36, 37, 40, 58, 65-68, 82, 90, 91, 94-96, 98).**

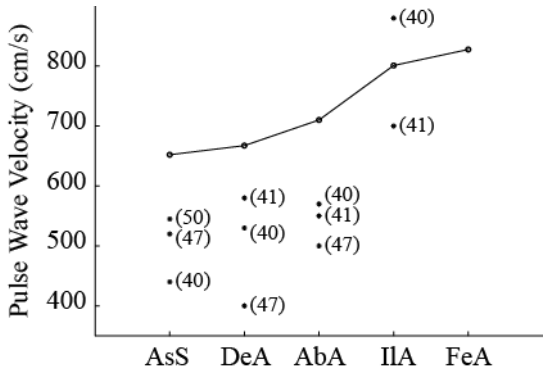


**Figure 10: Comparison between model predictions and reported values for pulse wave velocity, a composite mechanical property or arteries. Number next to data point denotes the relevant reference: (41, 42, 48, 51).**

## Discussions

*The Balance Point Approach Integrates Hemodynamics, Biomechanics, and Mechanobiology*. There has been a strong and growing interest in bridging the typically isolated fields of pulsatile hemodynamics, biomechanics and mechanobiology to relate altered hemodynamic variables to normal and pathological structures of elastic arteries (19, 35, 100, 101), networks of microvessels (71, 77, 78), and networks of conductance vessels (49, 111). The computational model developed in this chapter *simultaneously* predicted equilibrium arterial mechanical properties, pulsatile pressures and flows, and mechanical stresses in a human systemic arterial system (Fig. 2). Recapitulating the general principle of Cecchini et al. (11), the results in this chapter illustrate that a balance point approach (Fig. 3) makes the assumption of a set-point stress is entirely unnecessary and re-emphasizes a fundamental physiological concept: arterial adaptations must provide negative feedbacks to mechanical processes that leads to stable structural and mechanical equilibria. For instance, the positive value of $\alpha$ in *Eq. 16a* models an adaptive response that increases radius in response to increased endothelial shear stress (Fig. 3A, dashed line). An increase in radius in turn reduces shear stress, as illustrated by the mechanics curve in Fig. 3A (solid line). A useful result of eliminating the common assumption of a stress set point is that adaptive responses affecting radii, wall thicknesses and elastic moduli can be related to parameters directly related to mechanobiology ($\alpha$, $\beta$, $\gamma$). Another useful result of using this balance point approach is that the *teleological* argument used by West et al. (106) to explain the complex structure of the systemic arterial system can now be related to specific *mechanisms* leading to complex adaptive behavior.

*From "Design Principles" to "Self-Assembly Principles"*. Instead of invoking teleological design principles characterizing the *goals* of adaptation (57, 106), the mechanistic approach employed in this dissertation identifies "self-assembly principles" characterizing the *means*. 1) *Stability*: independently adapting vessels must achieve stable equilibrium despite their complex interactions. 2) *Efficiency of information transfer*: a relatively limited number of adaptive rules encoded within genes must generate innumerable of arterial structural properties. 3) *Adaptability*: the adaptive mechanisms that give rise to observed equilibrium properties must also allow the system to adapt to maintain proper function in response to perturbations. Analysis of the adaptability of the arterial system is the focus of Chapter V, and the clinical consequence of diminished adaptability is the focus of Chapter VI.

# CHAPTER V

# PULSE PRESSURE HOMEOSTASIS

## Problem Statement

Aortic pulse pressure emerges from the complex interaction of the heart, the systemic arterial system, and the peripheral circulations. Although conductance arteries are reported to adapt to changes in their local mechanical environment, the complexity of the cardiovascular system precludes the ability to experimentally relate vascular adaptive responses to changes in pulse pressure. Therefore, the purpose of this chapter is to the adaptive arterial system model developed in Chapter IV to test the hypothesis that global pulse pressure homeostasis can emerge from local adaptation of arteries to mechanical stresses.

## Methods

*Arterial Segment Compliances.* The compliance of each arterial segment in the model was calculated assuming a thick-walled vessel. Characterized elsewhere (61), it is a function of vessel radius, wall thickness, wall thickness, length ($l$), and elastic modulus.

$$C = \frac{3\pi r^2 (r+h)^2 l}{Eh(2r+h)} \qquad (18)$$

The total arterial compliance is the sum of the compliances of all 121 vessel segments. When mean pressure increases acutely, arterial compliance initially decreases. To characterize compliances after an initial perturbation, compliance per unit length ($C$) was

assumed to be a function of mean pressure ($\bar{P}$), where $C = ae^{b\bar{P}}$, with empirical constants *a* and *b* reported by Liu et al. (46).

*Adaptation to Reduced Pulsatility of Input Flow.* Adaptation to reduced pulsatility from the heart was simulated by reducing the amplitude of the input flow wave ($Q_p$) by 50% from the baseline value of 424 ml/s while maintaining the mean flow rate constant (Fig. 12A, dashed line). This magnitude of reduction in aortic pulsatile flow is consistent with the reported reduction of ejection fraction in patients with congestive heart failure (43, 56, 104). Arterial segments were then allowed to adapt according to *Eq. 20*, illustrated in Fig. 11.

*Adaptation to Increased Peripheral Resistances.* Adaptation to increased systemic vascular resistance was simulated by increasing the total peripheral resistance by 20% from baseline values of 0.8 mmHg·s/ml to acutely increase mean pressure to approximately 120 mmHg. This increase in total resistance is similar to the increase reported for ages 20 to 70 years (59). Arterial segments were then allowed to adapt according to *Eq. 20,* illustrated in Fig. 11.

*Adaptation to Aortic Narrowing.* A segment of the thoracic aorta (DeA, Fig. 1) was made narrow to explore arterial adaptation to an abrupt change in local mechanical properties. The radius of the vessel segment (5.2 cm in length) was reduced by 75% from the baseline value of 0.68 cm (i.e., aortic coarctation). The wall thickness and elastic modulus of this segment were held constant while the rest of the arterial segments of the model were allowed to adapt according to *Eq. 20,* illustrated in Fig. 11. For clarity, only adaptive changes in segments upstream and downstream along the aorta are reported.

*Realistic Adaptive Response to Coarctation: Aortic Narrowing and Reduced Peripheral Resistance.* Aortic coarctation, when it narrows the aorta enough to impact mean flow, typically induces dilation of downstream resistances. To simulate the possible microvascular adaptation to severe aortic coarctation in which mean flow is regulated, both the radius of a segment of the descending aorta was reduced by 75% (Fig. 1) and its downstream resistances also reduced by 40%. These concurrent changes were chosen such that the mean flow through the segment was maintained at the baseline value. The rest of the arterial segments were then allowed to adapt according to *Eq. 20*.

*Realistic Adaptive Response to Heart Failure: Reduced Cardiac Output and Increased Peripheral Resistance.* Arterial adaptation to reduced ejection fraction at constant mean arterial pressure was simulated by reducing the peak input flow by 50% (Fig. 12B, dashed line) while increasing peripheral resistances by 200%. These concurrent changes were chosen such that the mean aortic pressure was maintained at the baseline values. The arterial segments were then allowed to adapt according to *Eq. 20*.

*Graphical Analysis of Adaptation to Altered Hemodynamics.* To conceptualize the interaction of vascular biomechanics and adaptive responses, illustrative balance point graphs were constructed (11). In this case, the relationship of thoracic aortic radius and shear stress was analyzed. While all other parameters were held constant, two hemodynamic curves were constructed by varying the radius from 0.5 cm to 1.0 cm for the cases of 1) normal input flow, and 2) reduced pulsatility input flow. The adaptive curve was constructed by plotting *Eq. 16a* for the resulting range of $\tau_{rms}$.

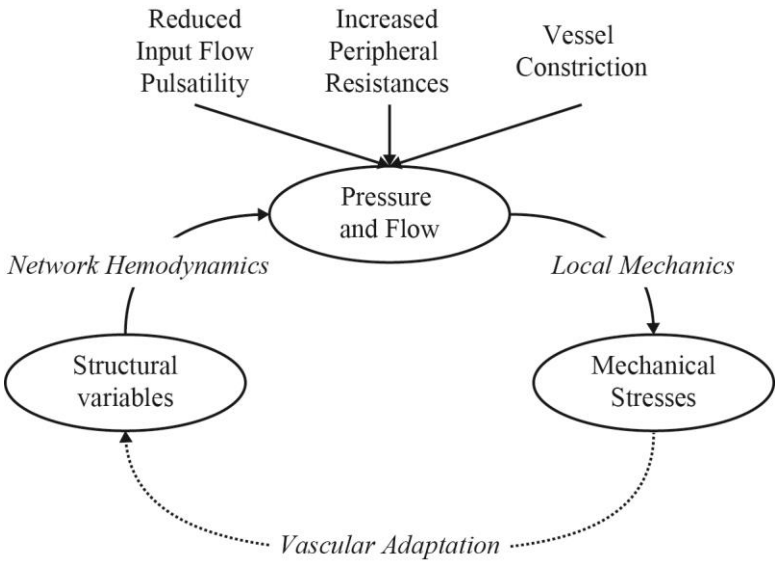


**Figure 11: Diagram of the interaction among structural variables (radius *r*, wall thickness *h*, and wall stiffness *E*), pressures and flows (*P* and *Q*), and mechanical stresses (wall circumferential stress $\sigma_{rms}$ and endothelial shear stress $\tau_{rms}$). The iterative process to calculate equilibrium variables ($r$, $h$, $E$, $P$, $Q$, $\sigma_{rms}$, $\tau_{rms}$) starts with assuming identical initial values of structural variables for all 121 vessel segments: $r$ = 1 mm, $h$ = 1 mm, and $E$ = 100 kPa.**

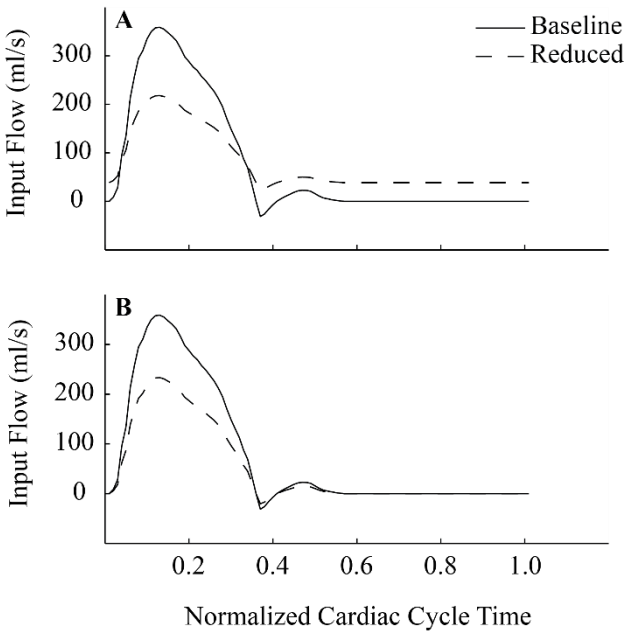


**Figure 12: A) Assumed input blood flow for baseline (solid curve) and for a reduction in pulsatility while cardiac output is maintained (dashed curve). Note that input flow is non-zero during diastole in order to keep the mean flow constant. B) Reduced peak flow and mean flow to simulate reduced ejection fraction.**

*Graphical Analysis of Adaptation of Vessels Upstream and Downstream of an Aortic Coarctation.* To conceptualize the complex adaptive responses to aortic coarctation, standard balance point graphs were constructed for vessels segments immediately upstream and downstream of the constricted segment. While all other parameters were held constant, the hemodynamic curve for the upstream vessel segment was plotted as the radius was varied from 0.5 cm to 1.0 cm. The corresponding adaptive curve was plotted from *Eq. 16a* for the corresponding change in $\tau_{rms}$. Similar hemodynamic and adaptation curves were established for the adaptation of wall thickness to $\sigma_{rms}$ by varying wall thickness from 0.05 cm to 0.15 cm, and for the adaptation of elastic modulus to $\sigma_{rms}$ by varying $E$ from 100 kPa to 1000 kPa. This procedure was repeated for the downstream segment.

**Results**

*Partial Restoration of Pulse Pressure and Shear Stress in Response to Reduced Pulsatility of Input Flow.* In response to a 50% reduction in input pulse flow, pulse pressures in all arteries acutely decreased from baseline (Fig. 13A). Because mean flow (and thus mean pressure) was maintained, there was no acute change in compliances (Fig. 13B). Adaptation increased pulse pressures towards baseline values (Fig. 13A) and decreased vessel compliances (Fig. 13B). These increase in pulse pressures and decreases in arterial compliances resulted from decreased radii, decreased wall thicknesses, and increased elastic moduli. The acute values of $\sigma_{rms}$ decreased compared to baseline, and the adaptive process further decreased equilibrium $\sigma_{rms}$ in all vessels. The acute values of $\tau_{rms}$

decreased from baseline in all vessels, but adaptive process increased equilibrium $\tau_{rms}$ towards baseline.

*Partial Restoration of Pulse Pressure and Mechanical Stresses in Response to Increased Peripheral Resistances.* In response to a 20% increase in peripheral resistances, pulse pressures in all vessels acutely increased (Fig. 13C). Mean pressure is acutely and chronically increased due to sustained elevation in peripheral resistances. Because mean pressure increased, the acute arterial compliances decreased (Fig. 13D). Adaptation caused pulse pressures to decrease back towards baseline values (Fig. 13C) and increased vessel compliances (Fig. 13D) from acute values. Furthermore, adaptation increased radii, increased wall thicknesses, and decreased elastic moduli in all vessels. The acute values of $\sigma_{rms}$ increased compared to baseline, but the adaptive process decreased equilibrium $\sigma_{rms}$ towards baseline. The acute values of $\tau_{rms}$ decreased from baseline in all vessels, but adaptive process increased equilibrium $\tau_{rms}$ towards baseline.

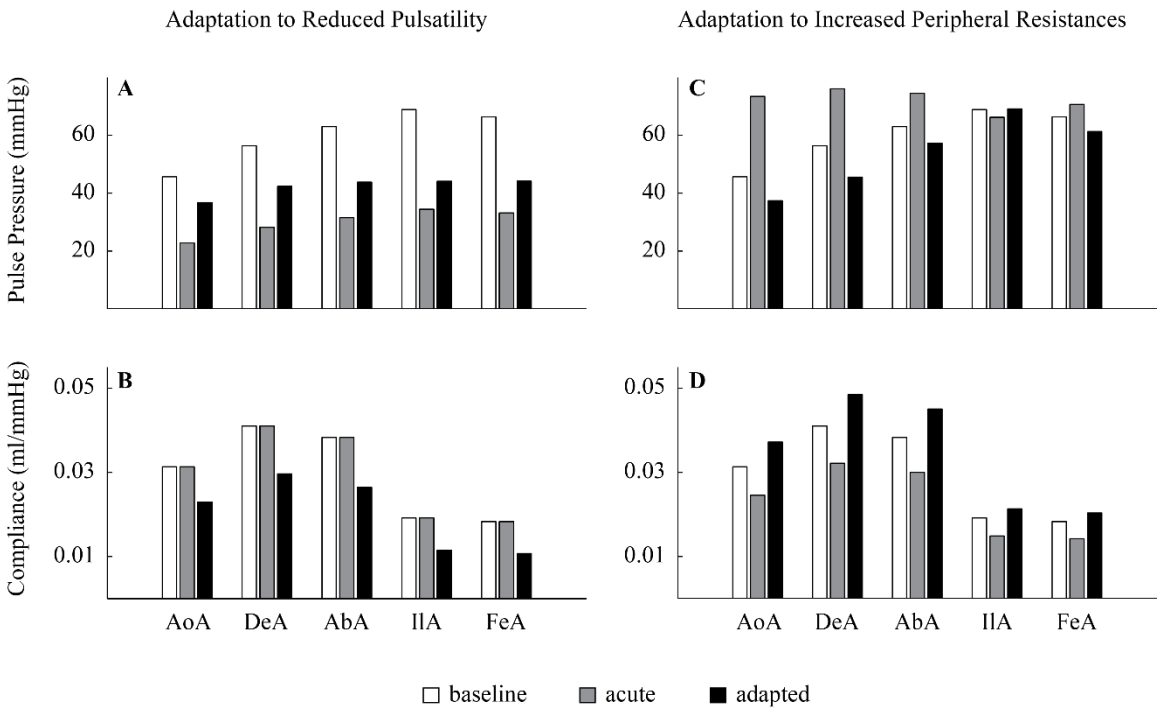


**Figure 13: Pulse pressure along the aortic-femoral pathway is restored towards baseline values in response to A) decreased input pulsatility and C) increased peripheral resistances. Associated with pressure homeostasis is B) a reduction in vessel compliances due to reduced pulsatility, and D) increased vessel compliances in due to increased peripheral resistances.**

*Adaptation of Vessels Upstream and Downstream to Aortic Narrowing.* Figure 5 illustrates that in response to a 75% decrease in lumen radius of a segment of the descending aorta (DeA), pulse pressure acutely increased in vessel segments upstream of the adaptation (AoA) and decreased in downstream vessels (AbA). The decrease in radius was sufficient to increase mean pressure upstream and decrease mean pressure downstream. Thus vessel compliance acutely decreased upstream and increased downstream (Fig. 14B). Adaptation reduced pulse pressure towards baseline in upstream vessels, but further reduced pulse pressure in downstream vessels (Fig. 14A). Adaptation increased arterial compliances upstream towards baseline, and decreased compliances downstream below baseline values (Fig. 14B). Furthermore, adaptation reduced radii in all vessels. Adaptation also increased wall thicknesses upstream and decreased them downstream. Adaptation decreased elastic moduli upstream and increased them downstream. In upstream vessels, $\sigma_{rms}$ acutely increased, and the process of adaptation decreased $\sigma_{rms}$ back towards baseline. In downstream vessels, $\sigma_{rms}$ acutely decreased, but the process of adaptation further decreased $\sigma_{rms}$. In all vessels, $\tau_{rms}$ acutely decreased, and the process of adaptation increased $\tau_{rms}$ back towards baseline.

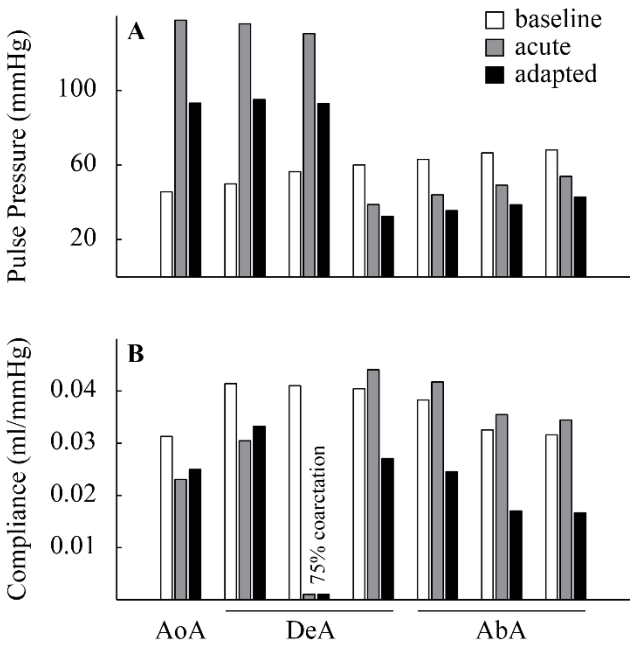


**Figure 14: Evidence of pulse pressure homeostasis in vessels upstream of narrowing of descending aorta (DeA, Fig. 1). A 75% reduction in vessel radius acutely increased pulse pressure upstream in of the coarctation site while decreasing pulse pressure downstream.**

*Realistic Adaptation of Vessels Upstream and Downstream of Coarctation with Reduced Peripheral Resistances.* Simulating coarctation by narrowing a segment of the aorta while maintaining flow yielded results similar to those obtained from aortic narrowing alone (Fig. 15). The resulting changes in stresses, however, were qualitatively different. The values of $\sigma_{rms}$ is acutely increased in upstream vessels and decreased in downstream vessels. Adaptation decreased $\sigma_{rms}$ towards baseline in upstream vessels and increased $\sigma_{rms}$ towards baseline in downstream vessels. The values of $\tau_{rms}$ are acutely and chronically decreased from baseline in all vessels.

*Realistic Adaptation to Simulated Heart Failure.* Simulating heart failure by decreasing pulsatile and mean input flow while maintaining mean pressure caused pulse pressure to acutely decrease in all vessels (Fig. 16A). Since mean arterial pressure was maintained, there was no acute change in arterial compliance. Adaptation increased pulse pressure towards baseline and decreased vessel compliances (Fig. 16B). Furthermore, adaptation caused vessel radii and wall thickness to decrease in all vessels. Adaptation caused elastic moduli to increase relative to baseline. The values of $\sigma_{rms}$ in all vessels were acutely decreased compared to baseline, and were further decreased by adaptation. The values of $\tau_{rms}$ were acutely decreased compared to baseline, and adaptation increased $\tau_{rms}$ back towards baseline.

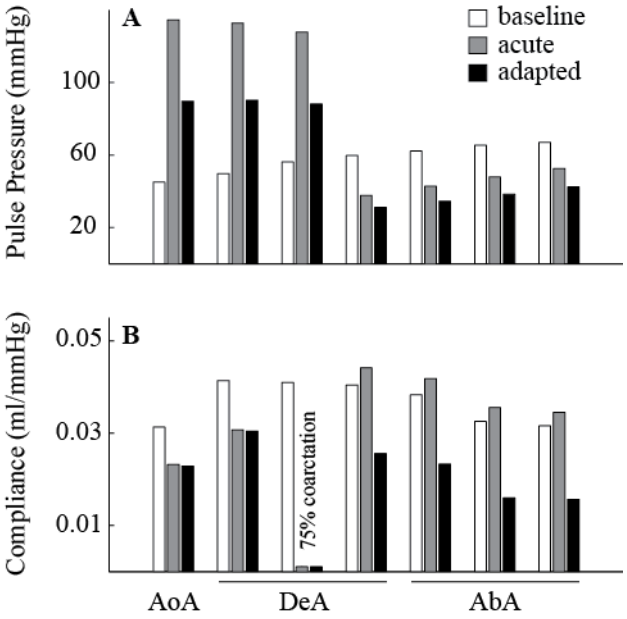


**Figure 15: Simulation of adaptation to descending aortic coarctation. Adaptation was simulated in response to a 75% coarctation with maintained mean flow. Pulse pressure in upstream vessel is reduced towards baseline after adaptation while compliance is reduced in all vessels.**

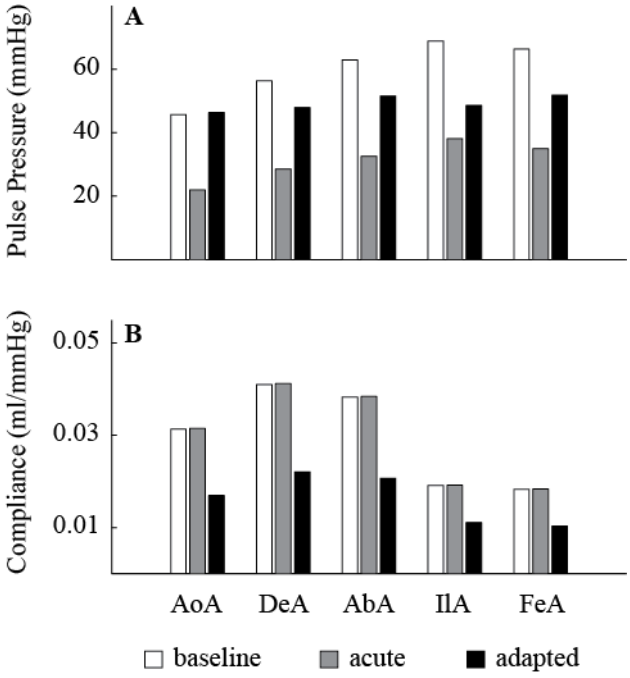


**Figure 16: Simulation of adaptation to heart failure. Adaptation to decreased pulse and mean input flow with increased peripheral resistance resulted in pulse pressure homeostasis in vessels along the aortic-femoral pathway.**

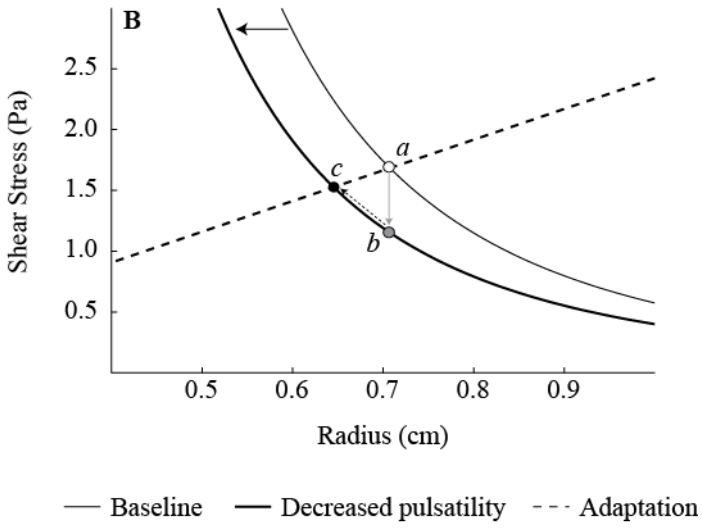


**Figure 17: Balance point for the local regulation of shear stress in response to decreased input pulsatility in the thoracic aorta. The biomechanics curves (solid lines) are characterized by *Eqs. 5* and *7*. The dashed line represents the adaptation curve characterized by *Eq. 16a*. The intersection (*point a*) represents the baseline equilibrium point. A decrease in input pulsatility necessarily shifts the mechanics curve to a lower shear stress (solid arrow). The initial shear stress before adaptation is represented by *point b*. Adaptation decreases radius and restores shear stress to a higher value (*point c*), albeit lower than baseline (point *a*).**

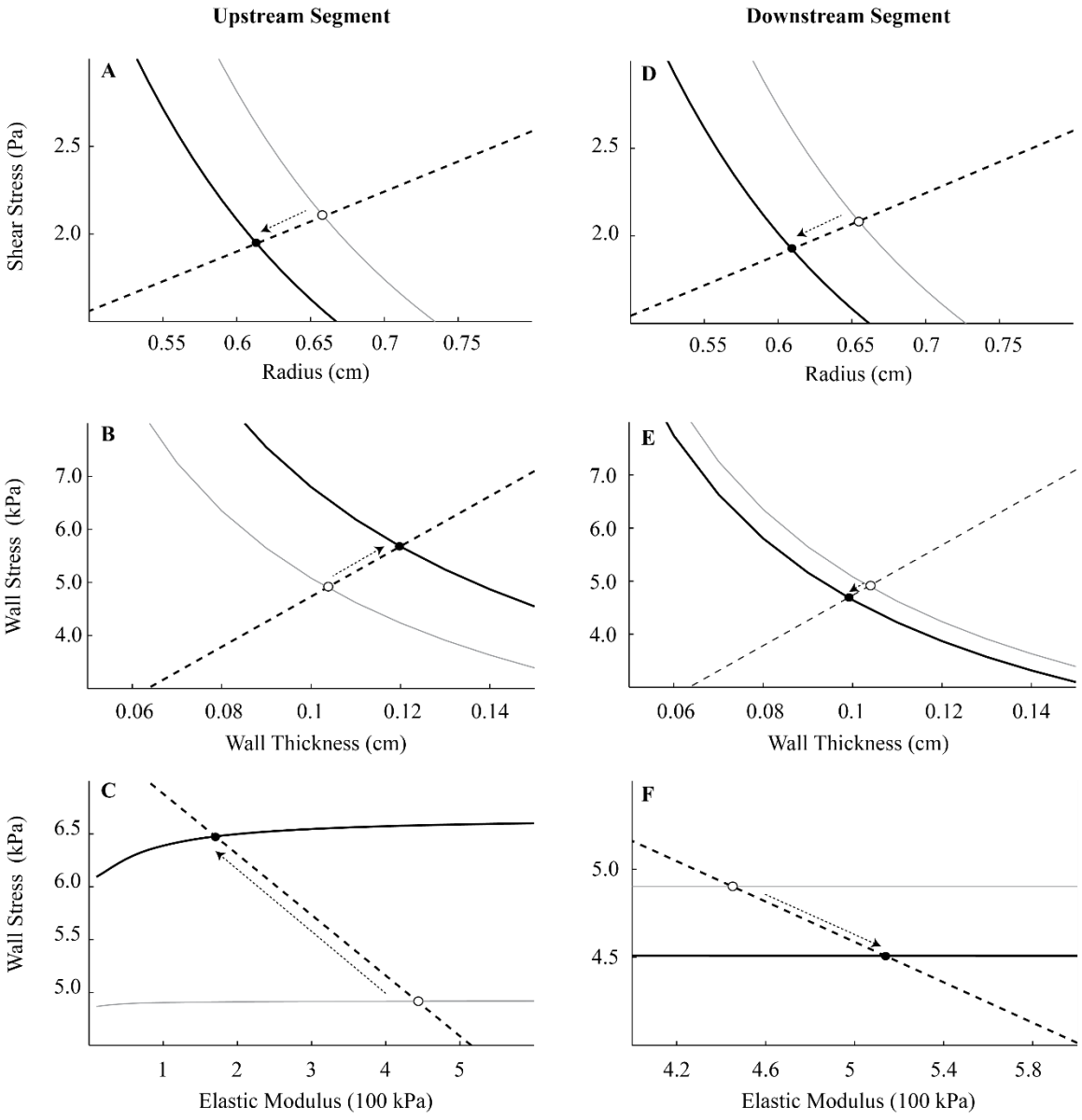


**Figure 18: Illustration of shift in equilibrium balance points in arterial segments upstream (*A*, *B*, *C*) and downstream (*D*, *E*, *F*) of aortic coarctation. Complexities in equilibrium arise from identical adaptive responses for upstream and downstream vessels responding to opposite changes in mechanical stresses: while the shift in the mechanics curves (solid lines) for radius and shear is in the same direction (*A*, *B*), the shift for wall thickness (*B*, *E*) and elastic modulus (*C*, *F*) are in opposite directions.**

**Discussions**

*Aortic Pulse Pressure Homeostasis Emerged from Simple Adaptive Rules Applied to A Realistic Human Systemic Arterial Network.* Adaptations of radii, wall thickness, and material stiffness act in concert to alter arterial compliances. A reduction in pulse pressure due to reduced pulsatility of input flow elicited an adaptive response that decreased arterial compliances and increased pulse pressure back towards baseline. An increase in pulse pressure due to increased peripheral resistances elicited an adaptive response that increased arterial compliances and decreased pulse pressure back to baseline. Finally, perturbations in pulse pressure due to reduction in radius of segment of the aorta elicited an adaptive response that increased compliance upstream causing upstream aortic pulse pressures to return toward baseline (Fig. 18). Adaptive response of the arterial network model to combinations of these perturbations to better simulate heart failure and aortic coarctation are also homeostatic. Using a mathematical modeling approach characterizing the means of adaptation, rather than prescribing an end to adaptation (i.e., *a priori* assumption of equilibrium stress set points or teleological goals), these emergent, homeostatic behaviors were directly attributable to fundamental hemodynamic and adaptive processes. From the simplicity of the assumptions employed, a new homeostatic mechanism could be identified: systemic pulse pressure regulation arises from adaptation of conductance arteries to local mechanical stimuli.

*Connecting Local Stress-Induced Arterial Adaptation to Pulse Pressure Homeostasis.* In this chapter, that radii, wall thicknesses, and material stiffnesses was assumed to adapt to local stresses (*Eq. 16*). Although each response provides negative

feedback to maintain vascular stresses, they also act to alter arterial segment compliance. In general, an increase in arterial compliances reduces pulse pressures (52, 59, 61). When pulsatile pressure increases, pulsatile wall stress increases, and wall stiffness decreases and wall thickness increases. These adaptations act antagonistically, increasing and decreasing arterial compliance, respectively (*Eq. 18*). The balance of the two opposing adaptive responses tends to increase compliance, a requirement to provide global feedback to lower pulsatile pressures. However, additional complexities in the results arose from the hemodynamics in networks (Fig. 18): 1) pressures in all vessels are affected by the sum of arterial compliances (61), 2) pulse pressure in each vessel segment is affected by arterial wave reflection, which depends on compliances, cross-sectional areas, and network architecture (7, 93), and 3) equilibrium pulse pressure and compliances of vessels are not determined by a single vessel, but rather the simultaneous adaptation of all vessels in the network. This chapter thus clarified a critical concept—information transfer by hemodynamic signals—is sufficient to coordinate independently arteries adapting to local stresses and yield global pulse pressure homeostasis.

*Judicious Use of Simplifying Assumptions Allowed Identification of Homeostatic Mechanisms.* A number of simplifying assumptions were made to characterize hemodynamic regulation by stress-induced arterial adaptation. First, linearity in the mathematical descriptions of pulsatile hemodynamics (61) and arterial adaptation was assumed, limiting the number of model parameters to only those describing fundamental behaviors. Second, the root-mean-square values (rather than steady or pulsatile values) were used to characterize stresses to the effects of both mean and pulsatile stresses. Third,

only adaptations to average values of endothelial shear stress and wall circumferential stress were assumed, minimizing unnecessary complications in the results by second-order effects such as longitudinal extension and torsion. Together, the assumptions retained tractability of the numerical simulations and allowed us to attribute complex, emergent behaviors to simple adaptive rules. While it was deemed that a representative set of three single perturbations and two combined perturbations were sufficient to delineate fundamental homeostatic responses illustrative perturbations, this work can be extended to simulate a number of other perturbations. The goal of chapter, however, was clarity over comprehensiveness.

*Balance Point Approach Captures Complexities in Network Hemodynamics and Adaptation.* Consistent with experimental results on chronic adaptation of arteries *in vivo* (50), the stresses on arteries, as well as pulse pressures and compliances, do not return to baseline in equilibrium in our results. The adaptive processes only reduce the initial perturbations. The basis for this incomplete restoration of stresses can be illustrated using the balance point graph in Fig. 17. The use of *finite* values for $\alpha$, $\beta$, or $\gamma$ prevents the adaptive process to return to *point a*, the baseline equilibrium point. Rather, a new equilibrium is achieved at *point c*. Increasing the gain of the adaptive processes (by increasing all three sensitivity parameters) to infinity results in vertical lines for the adaptation curves. An infinite gain reduces the system into one in which perturbations affects mechanical variables but not equilibrium stresses. The parameters for describing each adaptive response can be replaced with one: a target stress value. Assuming a set point stress thus removes the role of sensitivity of arterial radii, wall thickness, and

stiffness ($\alpha$, $\beta$, and $\gamma$) to vascular stresses from the model. These parameters are fundamental mechanobiology parameters, with $\alpha$ being the closest chronic analogue of the acute shear-induced dilation sensitivity measured *in vitro* (38, 44).

*Adaptive Model Predicted Fundamental Response of the Arterial System to External Perturbations*. While the perturbations were limited to simple mechanical perturbations, the fundamental predictions can be validated: an increase in pulse pressure leads to an adaptive response that decreases arterial compliances. This change in compliance has been well recognized, and is termed "compliance resetting" *in vivo* (16). While it is difficult to decouple pulsatile and mean pressure using experimental interventions, recent clinical interventions have revealed counterintuitive behaviors that are in agreement with our prediction. For instance, implantation of steady-flow left ventricular assist devices (LVAD), significantly reduces pulse pressure, and in many cases completely remove pulsatility from the arterial system (5, 99), leading to a decrease in arterial distensibility (97) and increased input impedance (5). In addition, in agreement with the clinical measurements by Arnold et al (1), our results for heart failure led to a counterintuitive reduction in vessel compliances (Fig. 16), and thus increased pulse wave velocity (*Eq*. 24). Our simulations, therefore, may provide a potential explanation for the observed constant pulse wave velocity in heart failure patients with reduced pulse pressure (25). Coarctation repair in children (47) as well as adults, reducing pulse pressure upstream, led to a decrease in aortic distensibility (64). Hence, while experimental evidence directly establishing the causal relationship changes in pulse pressure and wall

stiffness is scarce, the availability of clinical correlates gives us confidence in the validity of our predictions.

# CHAPTER VI

# ROLE OF DIMINISHED ARTERIAL ADAPTATION

## Problem Statement

Arterial hemodynamics is determined in part by arterial compliance, and measured pulse wave velocity and pulse pressure has been traditionally used as clinical indices of vascular health. Two classical models of the arterial system are traditionally used to relate these clinical indices to arterial mechanical properties: 1) the "infinitely long tube" model for analytically pulse wall stress and pulse wave velocity to the vessel mechanical properties, and 2) the Windkessel model for analytically relating global pulse pressure to total arterial compliance. Modern mechanobiology, however, has revealed that arteries respond and adapt to local mechanical stresses, and the mechanotransduction process can be influenced by disease states. The purpose of this chapter is use the "infinitely long tube" and Windkessel models, in addition to the computational model developed in Chapter IV, to test the hypothesis that diminished ability to adapt to pulsatile wall stress can cause arterial compliance to decrease, and pulse wave velocity and pulse pressure to increase.

## Methods

*Rule Describing Adaptation of Arteries to Pulsatile Wall Circumferential Stress.* The fundamental assumption of this chapter is that arterial wall stiffness adapts to circumferential wall stress. In particular, arteries adapt to the amplitude of the pulsatile wall circumferential stress ($\tilde{\sigma}$). To simplify, $\tilde{\sigma}$ was assumed to represent the stress

averaged over the wall thickness ($h$). According to Laplace's Law, $\tilde{\sigma}$ depends on a pulse pressure ($\tilde{P}$) and a radius ($r$), here assumed to be constant.

$$\tilde{\sigma} = \frac{r}{h}\tilde{P} \tag{19}$$

Consistent with the approached employed in this dissertation, the modulus of elasticity ($E$) was used to characterize vessel wall material stiffness and a linear equation was prescribed to mathematically model the adaptive response of $E$ to $\tilde{\sigma}$.

$$E = E_o - \gamma \cdot \tilde{\sigma} \tag{20}$$

The parameters $E_o$ and $\gamma$ are empirical parameters characterizing the adaptive response (*Eq. 20*). The value of $\gamma$ in particular characterizes the sensitivity of the arterial wall to pulse wall stress. Following previous chapters, the values of $E_o$ and $\gamma$ were assumed to be identical for all arteries in the systemic arterial system.

*Relating Pulse Wall Stress and Pulse Wave Velocity to Vessel Mechanical Properties in the Absence of Pulse Wave Reflection.* For analytical clarity, the classical model of an "infinitely long tube", which lacks pulse wave reflection, was used to characterize the relationship of local pulse pressure and mechanical properties of an elastic artery (61). The pulse pressure ($\tilde{P}$) is linearly proportional to the magnitude of the input flow ($Q_{in}$) and characteristic impedance ($Z_o$).

$$\tilde{P} = |Z_o| \cdot |Q_{in}| \tag{21}$$

The characteristic impedance is the vessel's input impedance when there is no pulse wave reflection. For a vessel with negligible resistance (appropriate for large elastic arteries), $Z_o$

may be approximated for a thin-walled vessel from the blood density ($\rho$), vessel geometry ($r$ and $h$), and elastic modulus ($E$) of the vessel wall (61).

$$Z_o = \frac{1}{\pi r^2}\sqrt{\frac{2\rho E h}{3r}} \tag{22}$$

Substitution of *Eqs. 22* and *21* into *Eq. 19* yielded a hemodynamic relationship for the pulse wall stress an artery as a function of the wall stiffness.

$$\tilde{\sigma}(\omega) = \frac{1}{\pi r}\sqrt{\frac{2\rho E}{3h}} \cdot |Q_{in}| \tag{23}$$

Assuming that the wall thickness is small compared to the vessel lumen radius, the finite pulse wave velocity ($c_o$) can also be approximated from values of $\rho$, $r$, $h$, and $E$ (61).

$$c_o = \sqrt{\frac{2Eh}{3\rho r}} \tag{24}$$

Standard balance point graphs were constructed to illustrate determinants of equilibrium $\tilde{\sigma}$ and $E$ as a result of the interaction of local mechanics (*Eq. 23*) and adaptive processes (*Eq. 20*) of a single vessel without reflection. The values of radius and wall thickness of the vessel were matched to the first segment of the descending aorta for the numerical model described in Chapter IV.

*Relating Pulse Pressure and Total Arterial Compliance in a Windkessel.* For analytical clarity, the classical two-element Windkessel model, which includes the effect of pulse wave reflection in stiff arterial systems, was used to characterize the relationship of global pulse pressure and total arterial compliance (61). Assuming that pulse wavelengths are sufficiently large that local structural variations are negligible, the Windkessel model assumes that pulse pressure ($\tilde{P}_W$) is rises and falls simultaneously

throughout the arterial system (53, 61). Analogous to the "infinitely long tube" model, $\tilde{P}_W$ is related to the magnitude of $Q_{in}$ by an input impedance ($Z_{in}$) rather than characteristic impedance (52, 61).

$$\tilde{P}_W = |Z_{in}| \cdot |Q_{in}| \tag{25}$$

The input impedance in turn depends on the total arterial compliance ($C_T$) and total systemic resistance ($R_S$) for each frequency ($\omega$).

$$Z_{in}(\omega) = \frac{R_S}{1 + j\omega R_S C_T} \tag{26}$$

The complex number $j = \sqrt{-1}$ represents the phase shift of each harmonic of the input impedance in the frequency domain. For each vessel $n$, the vessel compliance $C_n$ was computed from vessel geometry ($r$, $h$, and $E$) using a thin-walled approximation (61).

$$C_n = \frac{3\pi r_n^3 l_n}{2E_n h_n} \tag{27}$$

The total compliance is the sum of the vessel compliances of all $N$ vessels.

$$C_T = \sum_n^N \frac{3\pi r_n^3 l_n}{2E_n h_n} \tag{28}$$

Substitution of the adaptive rule (*Eq. 20*) into *Eq. 28* yields an expression for the total compliance as a function of the adaptive parameters and the pulse wall stress for each vessel ($\tilde{\sigma}$).

$$C_T = \sum_n^N \frac{3\pi r_n^3 l_n}{2(E_o - \gamma\tilde{\sigma}_n)h_n} \tag{29}$$

Noting that the sum of the volume of each vessel volume ($\pi r_n^2 l_n$) is equal to the volume of the entire arterial system ($V_B$), and assuming that the radius to wall thickness ratio remains relatively constant, an approximation for total compliance can be formulated.

$$C_T \approx \frac{3}{2}\frac{r}{h}\frac{1}{(E_o-\gamma\tilde{\sigma})}V_B = \frac{3}{2}\frac{r}{h}\frac{1}{\left(E_o-\gamma\tilde{P}_w\frac{r}{h}\right)}V_B \quad (30)$$

*Equation 12* thus approximates total arterial compliance that is consistent with "elastic tapering" (increasing in *E* with distance from the heart), assuming the pulse wall stress $\tilde{\sigma}$ is constant for all vessels. This assumption is equivalent to assuming that $\tilde{P}$ and *r/h* are equal in all vessels. Substituting *Eq. 20* into *Eq. 30*,

$$C_T \approx \frac{3}{2}\frac{r}{h}\frac{1}{\left(E_o-\gamma P_w\frac{r}{h}\right)}V_B \quad (31)$$

A standard balance point graph was constructed to illustrate determinants of equilibrium pulse pressure and total compliance as a result of the interaction between hemodynamics (*Eqs. 25 - 28*) and adaptation of the entire arterial system (*Eq. 29*).

*Numerical Predictions for Pulse Wave Velocity, Vessel Compliances, and Pulse Pressure Using an Adaptive, Computational Model.* To predict aortic pulse pressure ($\tilde{P}$) and total arterial compliance ($C_T$) in an adapting arterial system, the computational model developed in Chapters IV and V (Fig. 1) was simplified. In this chapter, the values of radii ($r_n$) and wall thickness ($h_n$) were kept constant at values reported by Westerhof et al. (107) for each of 121 arteries. For computational modeling, the assumption of a thin-walled vessel with negligible resistance was relaxed. Instead, vessel the compliance per unit length ($C'$), characteristic impedance ($Z_o$) and phase velocities ($c_{ph}$) were calculated using equations for thick-walled, resistive vessels using standard equations (107).

$$C' = \frac{3\pi r^2(r+h)^2}{Eh(2r+h)} \quad (32)$$

$$Z_o = \sqrt{\frac{j\omega L'+R'}{j\omega C'}} \quad (33)$$

$$c_{ph} = \frac{j\omega}{\sqrt{(j\omega L' + R')j\omega C'}} \quad (34)$$

The inertance per unit length $L'$ and resistance per unit length $R'$ characterize the longitudinal impedance to blood flow.

$$R' = \frac{8\mu}{\pi r^4} \quad (35)$$

$$L' = \frac{\rho}{\pi r^2} \quad (36)$$

The dynamic viscosity of blood $\mu$ and density of blood $\rho$ were assumed to be constant. The values of the parameters $E_o$ and $\gamma$ were prescribed to yield a pulse pressure of 35 mmHg at the aortic root. Structural, mechanical, and hemodynamic consequences of decreased sensitivity were predicted by reducing the sensitivity parameter $\gamma$ by 50%. A reduction of $\gamma$ by 50% and increase in peripheral resistances by 20% was used to model isolated systolic hypertension.

*Extending Analytical Approximations.* The analytical approximation for analytical solutions describing changes in arterial mechanical properties with adaptive processes involving radii, wall thickness, and elastic modulus was extended. As assumed in Chapters IV and V, radius was assumed to increase with shear stress ($\tau$), wall thickness increase with wall stress ($\sigma$), and elastic modulus with wall stress ($\sigma$).

$$r = r_o + \alpha \cdot \tau \quad (37a)$$

$$h = h_o + \beta \cdot \sigma \quad (37b)$$

$$E = E_o + \gamma \cdot \sigma \quad (37c)$$

**Results**

*Interaction between Local Mechanics and Arterial Adaptation Determines Equilibrium Wall Stress and Elastic Modulus.* While the elastic modulus of the arterial wall cannot affect the steady component of wall circumferential stress, its effects on pulse pressure modulate the pulsatile component of wall stress (*Eq. 2*). For a given input flow, an increase in $E$ increases $\sigma_p$ in the absence of wave reflection (Fig. 19, solid line). Arterial adaptation linearly decreases $E$ in response to an increase in $\sigma_p$ (Fig. 19, dashed line). The graphical solution of *Eqs*. *2*0 and *23* yielded stable equilibrium values for $\sigma_p$ and $E$ at the intersection of the mechanics curve (Fig. 19, solid line) and the adaptation curve (Fig. 19, dashed line) for positive values of $\rho$, $h$, $E_o$, and $\gamma$.

*Interaction between Hemodynamics and Simultaneous Adaptation of Arteries Determines Global Pulse Pressure and Total Arterial Compliance.* For a given input flow and total systemic resistance, an increase in arterial compliance always decrease pulse pressure (Fig. 20, solid line). Simultaneous adaptation of arteries to pulse pressure-induced pulse stress increases total arterial compliance (Fig. 20, dashed line). The graphical solution of *Eqs*. *25*, *26*, and *29* yielded a stable equilibrium values for $\tilde{P}_W$ and $C_T$ at the intersection of the hemodynamic curve (Fig. 20, solid line) and adaptation curve (Fig. 20, dashed line) for positive values of $\omega$, $R_S$, $l$, $E_o$, and $\gamma$.

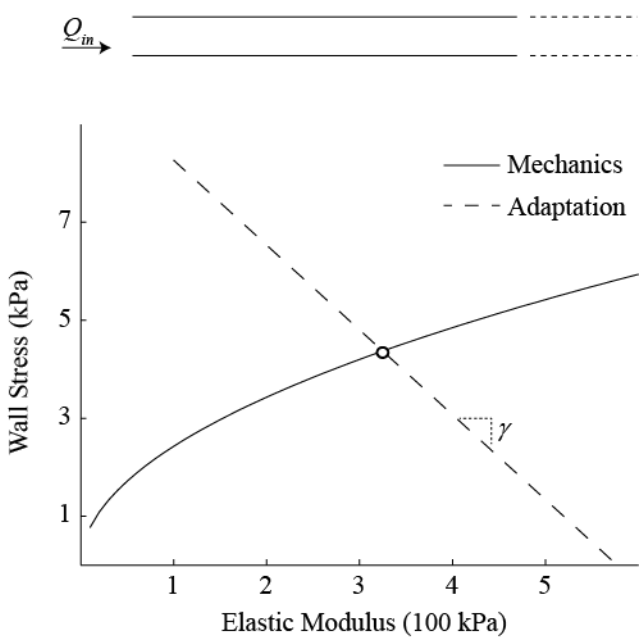


**Figure 19: Interaction between mechanics and vessel adaptation results in a stable equilibrium for the pulse wall stress ($\tilde{\sigma}$) and elastic modulus ($E$) of the vessel wall for an infinitely long tube. For a given input flow ($Q_{in}$), an increase in $E$ leads to an increase in $\tilde{\sigma}$ through increased pulse pressure (*Eq. 23*, solid line). The corresponding adaptive response (dashed line) reduces $E$ with increasing $\tilde{\sigma}$. The magnitude of the slope $\gamma$ of the adaptive curve represents the sensitivity of the arterial wall to pulse wall stress. The intersection between the mechanics and adaptation curves (circle) represents the equilibrium balance point.**

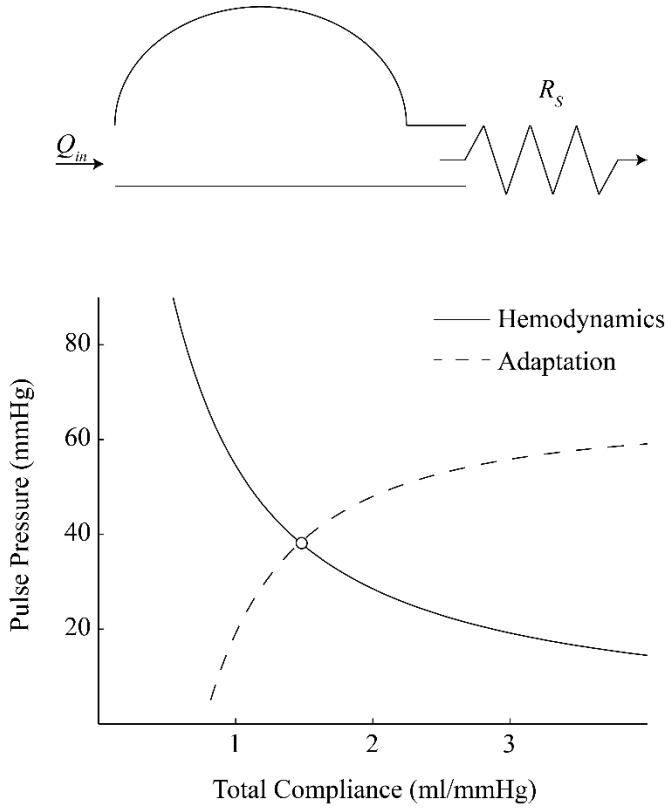


**Figure 20: Interaction between hemodynamics and arterial adaptation characterized by a classical Windkessel results in a stable equilibrium pulse pressure ($\widetilde{P}_W$) and total arterial compliance ($C_T$). For a given input flow ($Q_{in}$) and total systemic resistance ($R_s$), a decrease in $C_T$ leads to an increase in $\widetilde{P}_W$ (solid line). The corresponding adaptive response (dashed line) increases $C_T$ due to pulse pressure-induced increase in wall stress (*Eq. 20*). The intersection between the hemodynamic and adaptation (open circle) represents the equilibrium balance point.**

*Interactions between Mechanics, Hemodynamics, and Adaptation in a Distributed Network Determine Equilibrium Distributed Wall Stresses, Elastic Moduli, Pulse Pressures, and Vessel Compliances.* In the large distributed model (Fig. 21A), the effect of $E_D$ on $\sigma_D$ is smaller compared to that of $E$ on $\sigma_p$ for an infinitely long tube (Fig. 21B, solid line). Similarly, the hemodynamic relationship between $\tilde{P}_D$ and $C_T$ (Fig. 21C, solid line) exhibited complex variations in the distributed model. Applying the adaptive rule (*Eq. 20*) to a segment of the descending aorta of a distributed model of the arterial systemic circulation resulted in stable equilibria for pulse wall stress ($\sigma_D$), elastic modulus ($E_D$), pulse pressure ($\tilde{P}_D$), and total arterial compliance ($C_{DT}$) in the presence of wave reflection due to distributed network mechanical property and asymmetry.

*A Decrease the Sensitivity Parameter Shifts Equilibrium Variables to a New Steady State.* Reducing the value of $\gamma$ by 50% while keeping $E_o$ constant increased both the equilibrium value of $\sigma_p$ and $E$ in the absence of wave reflection (Fig. 22A). This increase resulted from a shift in the adaptive curve (Fig. 22A), resulting in a new equilibrium point (Fig. 22A, closed circle). The higher equilibrium value of $E$ necessarily results in a higher equilibrium characteristic impedance (*Eq. 22*), pulse wave velocity (*Eq. 24*), and vessel compliance (*Eq. 18*). In the Windkessel model, reducing $\gamma$ by 50% shifted the equilibrium point to a higher $\tilde{P}_W$ and lower $C_T$ (Fig. 22B, closed circle). The higher equilibrium value of $C_T$ necessarily results in a higher magnitude of arterial input impedance (*Eq. 26*).

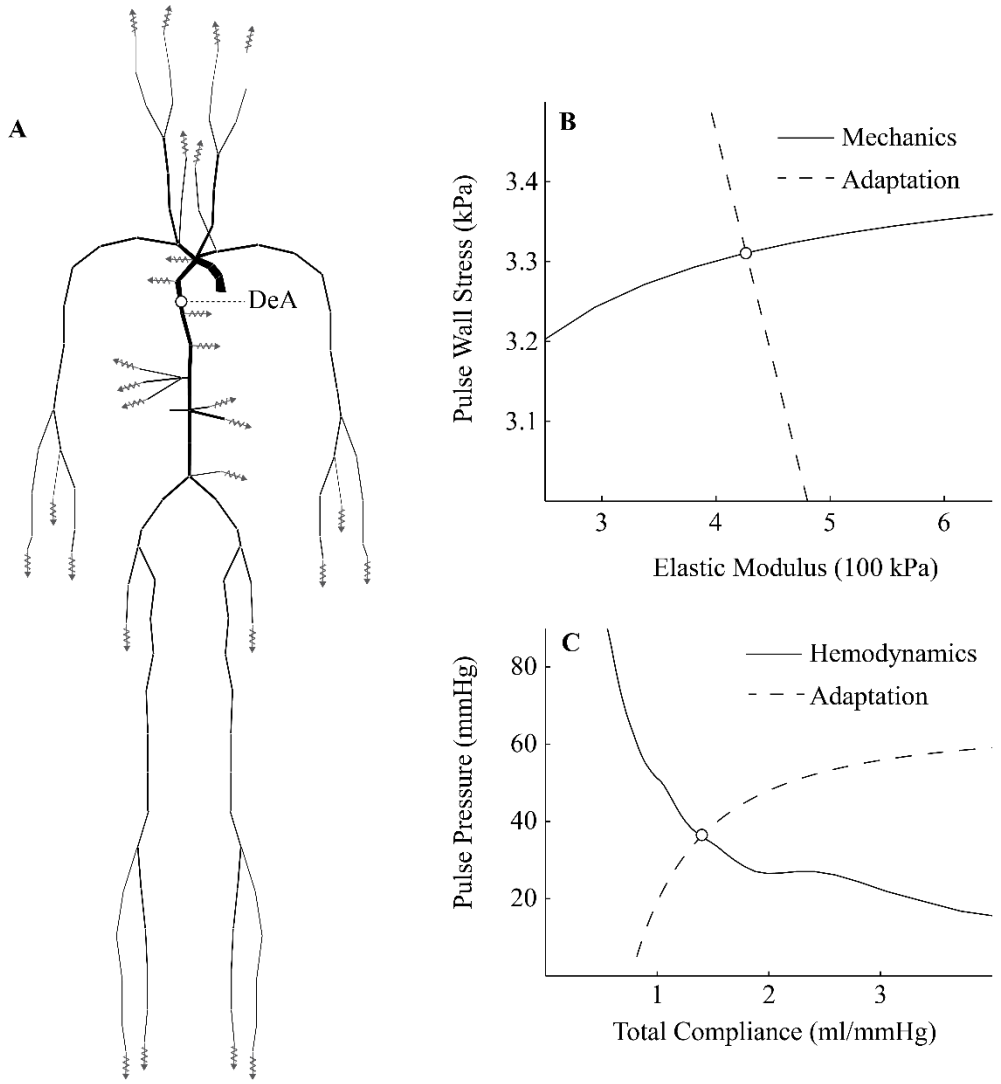


**Figure 21: A) Balance points for elastic modulus, pulse wall stress, pulse pressure, and total compliance for a segment of the descending aorta in a realistic network. B) Interactions between mechanics and adaptation in the descending aorta (DeA) results in local stable equilibria for pulse wall stress and elastic modulus. C) Interactions between hemodynamics and adaptation of all 121 arteries lead to a stable equilibrium between pulse pressure and total arterial compliance.**

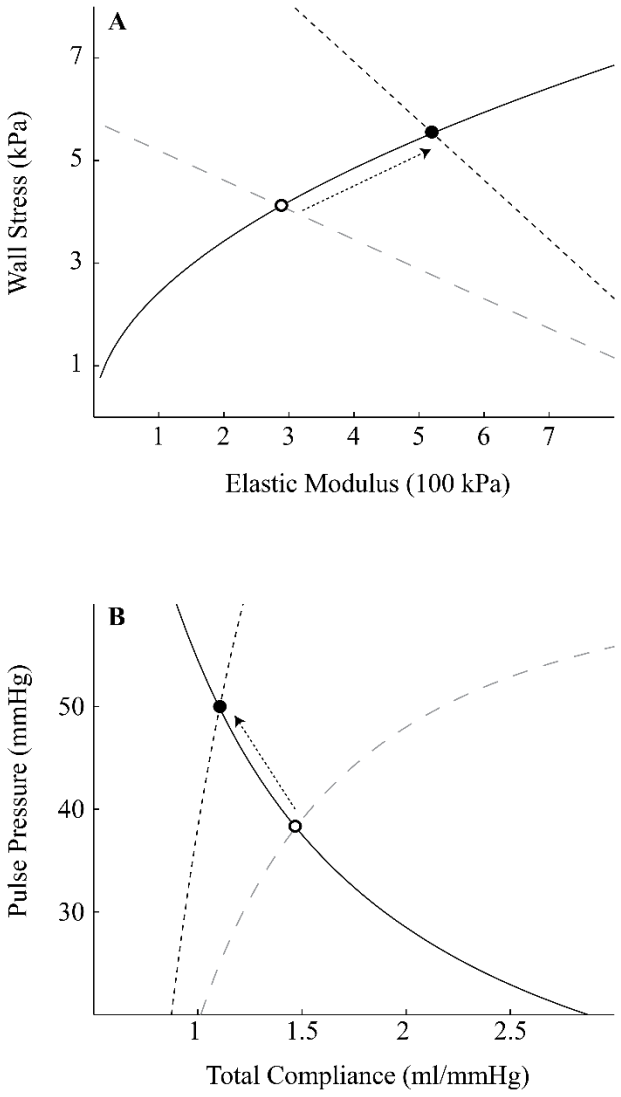


**Figure 22: A) Balance point of biomechanics and adaptation in a vessel with no pulse wave reflection. A 50% decrease in sensitivity to wall stress shifts the adaptive curve (arrow) from baseline (open circle) to a new equilibrium at a higher wall stress and elastic modulus (closed circle). B) Balance point of biomechanics and compliance adaptation in a classical Windkessel. A 50% decrease in sensitivity also shifts the equilibrium point for hemodynamics and adaptation (open circle) to a higher pulse pressure and lower compliance (closed circle).**

*Decreased Sensitivity Increases Pulse Wave Velocities and Decreases Vessel Compliances.* Applying the adaptive rule (*Eq*. 20), with $\gamma = 1.3 \times 10^{-5}$ (unitless) and $E_o = 10^3$ kPa resulted in stable, distributed equilibrium values for elastic moduli and pulse wall stresses, pulse pressures, and vessel compliances. The resulting total arterial compliance was 1.15 ml/mmHg, and the pulse pressure in the first segment of the descending aorta (Fig. 21, DeA) was 39.9 mmHg, with a diastolic pressure of 78.3 mmHg. A 50% decrease in $\gamma$ resulted in a decrease in total arterial compliance to 0.56 ml/mmHg with a corresponding increase in pulse pressure to 69.5 mmHg. In addition, pulse wave velocity in artery segments along the aorta, iliac artery, and femoral artery increased (Fig. 23A) due to a reduction in $\gamma$ while vessel compliance in the corresponding arteries increased (Fig. 23B).

*Decreased Sensitivity and Increased Peripheral Resistance Leads to Increased Mean and Systolic Pressure.* A decrease of g by 50% with an increase in systemic arterial resistance of 20% resulted in an increase in pulse pressure from 39.8 mmHg to 68.3 mmHg in the first segment of the descending aorta. While diastolic pressure increased by 4.5% from 78.3 mmHg in baseline (Fig. 24, solid line), systolic pressure increased from 118 mmHg in baseline to 150 mmHg. The pressure morphology for both cases are reported in Fig. 24.

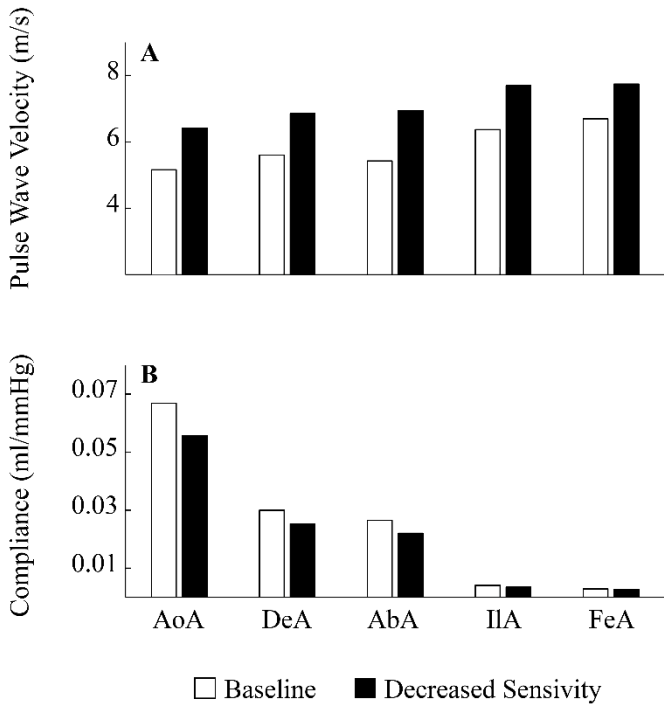


**Figure 23: A) Increase in pulse wave velocities due to a 50% decrease in sensitivity of adaptation ($\gamma$) in segments of the ascending aorta (AoA), descending aorta (DeA), abdominal aorta (AbA), iliac artery (IlA), and femoral artery (FeA). B) Decreased vessel compliance due to a 50% decrease in sensitivity in the same vessel segments along the aortic-femoral pathway.**

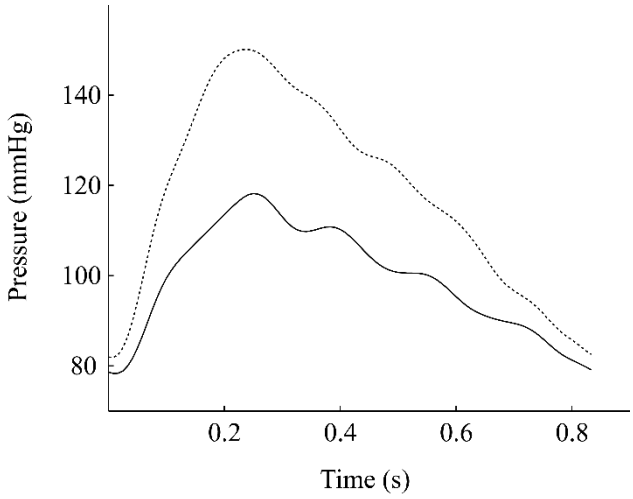


**Figure 24: Demonstration of isolated systolic hypertension due to a 50% percent decrease in sensitivity and 20% increase in peripheral resistance (dotted line) in the first segment of the descending aorta of the distributed model illustrated in Fig. 1. While diastolic pressure remains relatively constant compared to baseline (solid line), systolic pressure significantly increased.**

*Infinite Solutions for Parameters Describing Simultaneous Adaptation of Radius, Wall Thickness, and Elastic Modulus to Mechanical Stresses.* Substitution of *Eqs. 37* in to *Eqs. 18* and *24* yielded functional forms relating adaptive parameters for pulse wave velocity and compliance ($C_v$) of a vessel.

$$c_o = \sqrt{\frac{2(h_o+\beta\sigma)(E_o-\gamma\sigma)}{3\rho(r_o+\alpha\tau)}} \tag{38}$$

$$C_v = \frac{3\pi(r_o+\alpha\tau)^3 l}{2(h_o+\beta\sigma)(E_o-\gamma\sigma)} \tag{39}$$

When the radius-to-wall thickness ratio is constant, and if changes in arterial blood volume due to adaptation is small, the total compliance is analytical function of $\alpha$, $\beta$, and $\gamma$.

$$C_T \approx \frac{3(r_o+\alpha\tau)}{2(h_o+\beta\sigma)(E_o-\gamma\sigma)} V_B \tag{40}$$

For the special case of $r_o = 0$ and $h_o = 0$, *Eqs. 38 - 40* simplify.

$$c_o = \sqrt{\frac{2}{3\rho}\frac{\sigma}{\tau}\left(\frac{\beta E_o}{\alpha} - \frac{\gamma\beta}{\alpha}\sigma\right)} \tag{41}$$

$$C_v = \frac{3\pi l}{2}\frac{\tau^3}{\sigma}\left(\frac{\beta E_o}{\alpha^3} - \frac{\gamma\beta}{\alpha^3}\sigma\right)^{-1} \tag{42}$$

$$C_T = \frac{3V_B}{2}\frac{\tau}{\sigma}\left(\frac{\beta E_o}{\alpha} - \frac{\gamma\beta}{\alpha}\sigma\right)^{-1} \tag{43}$$

The ratios $\beta E_o/\alpha$ and $\gamma\beta/\alpha$ indicate infinite solutions for $\alpha$, $\beta$, $\gamma$, for measured equilibrium pulse wave velocity, vessel compliance, and total compliance.

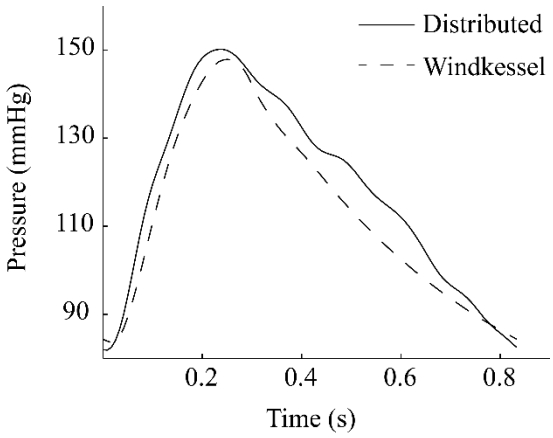


**Figure 25: Windkessel approximation for 50% loss of sensitivity and 20% increase in peripheral resistances. The two-element Winkessel approximation (dashed line) underestimated pulse pressure by 6.2% compared to the large-scale, distributed model (solid line).**

**Discussions**

*Isolated Systolic Hypertension Arises From Diminished Sensitivity to Vascular Wall Stress.* This chapter employed a simple adaptive rule to relate changes in mechanotransduction to changes in vascular mechanical properties, hemodynamics and stresses at multiple levels. Three classical models of the systemic arterial system were used to illustrate the consequence of losing sensitivity of the adaptive response to wall circumferential stress on elastic modulus, pulse wave velocity, total arterial compliance, and pulse pressure. First, in a single vessel without pulse wave reflection (Fig. 19B), diminished sensitivity led to increased pulse wall stress, increased material stiffness, and increased pulse wave velocity (*Eq. 24*). Second, in an entire arterial system acting as a classical two-element Windkessel (Fig. 20B), diminished sensitivity increased pulse pressure, decreased total arterial compliance, and increased input impedance (*Eq. 26*). Finally, algebraic predictions for aortic elastic modulus, pulse wall stress, pulse wave velocity, total arterial compliance, and aortic pulse pressure were using the computational model developed in Chapter IV. The increase in pulse wave velocity causes the arterial system to degenerate into a classical two-element Windkessel, where total peripheral resistance and total arterial compliance dominate the dynamic aortic pressure-flow relationship (53, 61). Since an adaptive arterial system reproduces the phenomena of "compliance resetting", where increases in mean pressure leads to adaptive responses that act to increase arterial compliance, an increase in total peripheral resistance alone does not increase pulse pressure (Fig. 13). However, when coupled with diminished sensitivity to circumferential wall stress, compliance decreases, and the model reproduces isolated

systolic hypertension (Fig. 24). This model thus reproduces the correlation of diminished compliance and pulse pressure, without having to make the untenable assumption inherent in fatigue theory that increased cyclical stress increases arterial stiffness. In this chapter, a decrease in 50% of the sensitivity to wall stress, coupled with a 20% increase in peripheral resistances, reduced the total arterial compliance of a large, distributed network from 1.15 ml/mmHg to 0.56 ml/mmHg, and pulse wave velocity in the descending aorta increased from 5.1 m/s to 6.4 m/s. The resulting pulse pressure in the descending aorta predicted using the distributed model was only 6.2% different than that of a Windkessel model (Fig. 25). While a high sensitivity parameter models the vascular dynamics of a young, healthy, normotensive individual, the current work illustrates that in isolated hypertension in the elderly the Windkessel model is sufficient to describe the arterial system.

*Biomechanics and Mechanobiology Inverse Problems*. In Chapters IV and V, simultaneous adaptation of radius, wall thickness, and material stiffness in the systemic arterial system was shown to result in stable equilibria for all structural, mechanical, and hemodynamic variables. These approaches in these previous reports can be characterized as "forward" problems, where all mechanisms, including values of adaptive parameters are known, and the variables of interest are calculated. The results required a numerical solution (with results expressed in graphs) that made it difficult to conceptualize how the adaptive responses interacted. However, both measurements of pulse wave velocity and total arterial compliance have been used to infer changes in vascular functions (52, 59). This approach, inferring mechanism and parameter values from measured variables, is

often termed the “inverse problem”. Inverse problems are common in clinical research. For instance, investigators attempt solve the “hemodynamic inverse problem” to capture total arterial compliance (79) from measured blood pressure and flows. Both changes in total arterial compliance and local arterial compliance have been used to infer the health of blood vessels in general (8-10), and vascular adaptive responses in particular (2, 88). Nonetheless, previous reports have illustrated that there are infinite solutions to the hemodynamic inverse problem, meaning the same measured blood pressures and flows could arise from different arterial compliances (79). This chapter relied on the fact that the arterial system degenerates into a Windkessel to extend the algebraic approximations to include the additional effects of adaptation of radii to endothelial shear stress (*Eq. 37a*) and wall thickness to wall stress (*Eq. 37b*). The combined adaptive rules illustrate the dependence of pulse wave velocity (*Eq. 38*), vessel compliance (*Eq. 39*) and total compliance (*Eq. 40*) on all adaptive parameters and their corresponding stimuli. These algebraic simplifications clarify the potential interactions of adaptive responses affecting local and total arterial compliances. While it is clear the hemodynamic inverse problem could be solved uniquely for total compliances (76), there are multiple potential adaptive responses that can lead to the same total arterial compliance. Thus, there are infinite solutions to the mechanobiology inverse problem, and thus, attempts to infer health of particular adaptive responses from measured equilibrium compliances and pulse wave velocity are futile.

# CHAPTER VII

# CONCLUSIONS

## Characterizing Hemodynamics and Mechanobiology Interactions

There has been a strong and growing interest in bridging the typically isolated fields of pulsatile hemodynamics, biomechanics and mechanobiology to relate altered hemodynamic variables to normal and pathological structures of elastic arteries (19, 35, 100, 101), networks of microvessels (71, 77, 78), and networks of conductance vessels (49, 111). Towards this end, investigators in the past have relied on *teleological* arguments to explain the origin of the normal vasculature (57, 106, 110, 112), as well as *homeostatic* stresses to explain vascular adaptation to external perturbations (49, 71, 73, 78). Chapters IV and V demonstrated that neither was necessary to predict the normal vascular network and responses of the normal arterial system to external perturbations. Only three adaptive responses based on experimental observations for radius, wall thickness, and elastic modulus was sufficient to predict distributed properties and a myriad of responses. This dissertation integrated changes in the mechanotransduction process to describe changes in arterial system dynamics. A shift in equilibrium, representing chronic, stable changes in arterial structural mechanical properties, hemodynamics, and stresses were directly related to parameters describing sensitivity of the adaptive response ($\gamma$). Finally, disease at the global level (isolated systolic hypertension) could be related to a derangement in cellular mechanotransduction. The current theoretical framework therefore fully integrates the

arterial network at the macroscopic (vessel) level to describe arterial system dynamics in terms of changes in mechanobiology within the context of network hemodynamics.

**Arterial Adaptation to Mechanical Stress Simultaneously Can Meet Many Demands**

Not only are pulse pressures and vascular stresses maintained with relatively narrow ranges in response to perturbations, they are relative constant across mammalian species. The most popular of the teleological explanations are that the systemic arterial system minimizes energy dissipation (57) and maintains optimal vascular stresses (112). Murray (57) predicted vascular branching patterns based on the assumption that the vascular system minimized energy dissipation. Zamir arrived at the same predicted geometries assuming that endothelial shear stresses in all vessels of a branch are constant (112). Whether the arterial system is energy efficient (34, 57, 106, 110) or maintains stresses within acceptable ranges (13, 28), vascular adaptation within a particular species may meet several demands. Previous attempts to predict the mechanical properties of arterial networks have assumed teleological principles (34, 57, 106, 110). The mechanistic assumptions (*Eq. 16*) do tend to minimize energy dissipation and maintain stresses within narrow ranges. Furthermore, these simple adaptive responses were assumed to apply to all arterial segments, thus eliminating the need for genetically encoding a large amount of information to achieve and maintain optimality. Whether these adaptive responses are conserved and provide a mechanistic basis for mammalian similarity and numerous reported allometric relationships (14, 15, 87, 108) remains an intriguing question.

## REFERENCES


1. Arnold JM, Marchiori GE, Imrie JR, Burton GL, Pflugfelder PW, and Kostuk WJ. Large artery function in patients with chronic heart failure. Studies of brachial artery diameter and hemodynamics. *Circulation* 84: 2418-2425, 1991.

2. Arrebola-Moreno AL, Laclaustra M, and Kaski JC. Noninvasive assessment of endothelial function in clinical practice. *Rev Esp Cardiol (Engl Ed)* 65: 80-90, 2012.

3. Astrand H, Ryden-Ahlgren A, Sandgren T, and Lanne T. Age-related increase in wall stress of the human abdominal aorta: an in vivo study. *Journal Of Vascular Surgery* 42: 926-931, 2005.

4. Astrand H, Sandgren T, Ahlgren AR, and Lanne T. Noninvasive ultrasound measurements of aortic intima-media thickness: implications for in vivo study of aortic wall stress. *Journal Of Vascular Surgery* 37: 1270-1276, 2003.

5. Bartoli CR, Giridharan GA, Litwak KN, Sobieski M, Prabhu SD, Slaughter MS, and Koenig SC. Hemodynamic responses to continuous versus pulsatile mechanical unloading of the failing left ventricle. *ASAIO Journal* 56: 410-416, 2010.

6. Berger DS and Li JK. Concurrent compliance reduction and increased peripheral resistance in the manifestation of isolated systolic hypertension. *The American Journal Of Cardiology* 65: 67-71, 1990.

7. Berger DS, Li JK, Laskey WK, and Noordergraaf A. Repeated reflection of waves in the systemic arterial system. *The American Journal Of Physiology* 264: H269-281, 1993.

8. Besouw MT, Holewijn S, Levtchenko EN, and Janssen MC. Non-invasive measurements of atherosclerosis in adult cystinosis patients. *Journal Of Inherited Metabolic Disease* 34: 811-818, 2011.

9. Blacher J, Guerin AP, Pannier B, Marchais SJ, and London GM. Arterial calcifications, arterial stiffness, and cardiovascular risk in end-stage renal disease. *Hypertension* 38: 938-942, 2001.

10. Boutouyrie P. New techniques for assessing arterial stiffness. *Diabetes & Metabolism* 34 Suppl 1: S21-26, 2008.

11. Cecchini AB, Melbin J, and Noordergraaf A. Set-point: is it a distinct structural entity in biological control? *Journal Of Theoretical Biology* 93: 387-394, 1981.

12. Cheng CP, Herfkens RJ, and Taylor CA. Abdominal aortic hemodynamic conditions in healthy subjects aged 50-70 at rest and during lower limb exercise: in vivo quantification using MRI. *Atherosclerosis* 168: 323-331, 2003.

13. Chien S. Mechanotransduction and endothelial cell homeostasis: the wisdom of the cell. *American Journal Of Physiology: Heart And Circulatory Physiology* 292: H1209-1224, 2007.

14. Dawson TH. Allometric relations and scaling laws for the cardiovascular system of mammals. *Systems* 2: 168-185, 2014.

15. Dawson TH. Similitude in the cardiovascular system of mammals. *The Journal Of Experimental Biology* 204: 395-407, 2001.

16. Drzewiecki G and Pilla JJ. Noninvasive measurement of the human brachial artery pressure-area relation in collapse and hypertension. *Annals Of Biomedical Engineering* 26: 965-974, 1998.

17. Folkow B. Structural factors: the vascular wall. Consequences of treatment. *Hypertension* 5: III58-62, 1983.

18. Folkow B. Structure and function of the arteries in hypertension. *American Heart Journal* 114: 938-948, 1987.

19. Fridez P, Rachev A, Meister JJ, Hayashi K, and Stergiopulos N. Model of geometrical and smooth muscle tone adaptation of carotid artery subject to step change in pressure. *American Journal Of Physiology Heart And Circulatory Physiology* 280: H2752-2760, 2001.

20. Fung YC. *Biomechanics : Circulation*. New York: Springer, 1997.

21. Gaenzer H, Neumayr G, Marschang P, Sturm W, Kirchmair R, and Patsch JR. Flow-mediated vasodilation of the femoral and brachial artery induced by exercise in healthy nonsmoking and smoking men. *Journal Of The American College Of Cardiology* 38: 1313-1319, 2001.

22. Girerd X, London G, Boutouyrie P, Mourad JJ, Safar M, and Laurent S. Remodeling of the radial artery in response to a chronic increase in shear stress. *Hypertension* 27: 799-803, 1996.

23. Gleason RL, Gray SP, Wilson E, and Humphrey JD. A multiaxial computer-controlled organ culture and biomechanical device for mouse carotid arteries. *Journal Of Biomechanical Engineering* 126: 787-795, 2004.

24. Gruionu G, Hoying JB, Pries AR, and Secomb TW. Structural remodeling of the mouse gracilis artery: coordinated changes in diameter and medial area maintain circumferential stress. *Microcirculation* 19: 610-618, 2012.

25. Guerin AP, Blacher J, Pannier B, Marchais SJ, Safar ME, and London GM. Impact of aortic stiffness attenuation on survival of patients in end-stage renal failure. *Circulation* 103: 987-992, 2001.

26. Guyton AC. Determination of cardiac output by equating venous return curves with cardiac response curves. *Physiological Reviews* 35: 123-129, 1955.

27. Hirata K, Triposkiadis F, Sparks E, Bowen J, Wooley CF, and Boudoulas H. The Marfan syndrome: abnormal aortic elastic properties. *Journal of the American College of Cardiology* 18: 57-63, 1991.

28. Humphrey JD. Vascular adaptation and mechanical homeostasis at tissue, cellular, and sub-cellular levels. *Cell Biochemistry And Biophysics* 50: 53-78, 2008.

29. Humphrey JD and Delange SL. *An Introduction to Biomechanics*: New York: Springer-Verlag, 2004.

30. Intengan HD and Schiffrin EL. Structure and mechanical properties of resistance arteries in hypertension: role of adhesion molecules and extracellular matrix determinants. *Hypertension* 36: 312-318, 2000.

31. Jankovski A, Francotte F, Vaz G, Fomekong E, Duprez T, Van Boven M, Docquier MA, Hermoye L, Cosnard G, and Raftopoulos C. Intraoperative magnetic resonance imaging at 3-T using a dual independent operating room-magnetic resonance imaging

suite: development, feasibility, safety, and preliminary experience. *Neurosurgery* 63: 412-424; discussion 424-416, 2008.

32. Jankowski P, Kawecka-Jaszcz K, Czarnecka D, Brzozowska-Kiszka M, Styczkiewicz K, Loster M, Kloch-Badelek M, Wilinski J, Curylo AM, Dudek D, Aortic Blood P, and Survival Study G. Pulsatile but not steady component of blood pressure predicts cardiovascular events in coronary patients. *Hypertension* 51: 848-855, 2008.

33. Kamiya A, Bukhari R, and Togawa T. Adaptive regulation of wall shear stress optimizing vascular tree function. *Bulletin Of Mathematical Biology* 46: 127-137, 1984.

34. Karreman G. Some contributions to the mathematical biology of blood circulation: Reflections of Pressure Waves in the Arterial System. *Bulletin of Matheamtical Biology* 14: 327-350, 1952.

35. Karsaj I and Humphrey JD. A Multilayered Wall Model of Arterial Growth and Remodeling. *Mechanics Of Materials : An International Journal* 44: 110-119, 2012.

36. Kawasaki T, Sasayama S, Yagi S, Asakawa T, and Hirai T. Non-invasive assessment of the age related changes in stiffness of major branches of the human arteries. *Cardiovascular Research* 21: 678-687, 1987.

37. Kornet L, Hoeks AP, Lambregts J, and Reneman RS. Mean wall shear stress in the femoral arterial bifurcation is low and independent of age at rest. *Journal of vascular research* 37: 112-122, 2000.

38. Kuo L, Davis MJ, and Chilian WM. Longitudinal gradients for endothelium-dependent and -independent vascular responses in the coronary microcirculation. *Circulation* 92: 518-525, 1995.

39. Lakatta EG. Hemodynamic adaptations to stress with advancing age. *Acta medica Scandinavica Supplementum* 711: 39-52, 1986.

40. Lanne T, Sonesson B, Bergqvist D, Bengtsson H, and Gustafsson D. Diameter and compliance in the male human abdominal aorta: influence of age and aortic aneurysm. *European Journal Of Vascular Surgery* 6: 178-184, 1992.

41. Latham RD, Westerhof N, Sipkema P, Rubal BJ, Reuderink P, and Murgo JP. Regional wave travel and reflections along the human aorta: a study with six simultaneous micromanometric pressures. *Circulation* 72: 1257-1269, 1985.

42. Learoyd BM and Taylor MG. Alterations with age in the viscoelastic properties of human arterial walls. *Circulation Research* 18: 278-292, 1966.

43. Letsou GV, Pate TD, Gohean JR, Kurusz M, Longoria RG, Kaiser L, and Smalling RW. Improved left ventricular unloading and circulatory support with synchronized pulsatile left ventricular assistance compared with continuous-flow left ventricular assistance in an acute porcine left ventricular failure model. *The Journal Of Thoracic And Cardiovascular Surgery* 140: 1181-1188, 2010.

44. Liao JC and Kuo L. Interaction between adenosine and flow-induced dilation in coronary microvascular network. *The American Journal Of Physiology* 272: H1571-1581, 1997.

45. Lim MA and Townsend RR. Arterial compliance in the elderly: its effect on blood pressure measurement and cardiovascular outcomes. *Clinics In Geriatric Medicine* 25: 191-205, 2009.

46. Liu Z, Brin KP, and Yin FC. Estimation of total arterial compliance: an improved method and evaluation of current methods. *The American Journal Of Physiology* 251: H588-600, 1986.

47. Lombardi KC, Northrup V, McNamara RL, Sugeng L, and Weismann CG. Aortic stiffness and left ventricular diastolic function in children following early repair of aortic coarctation. *The American Journal Of Cardiology* 112: 1828-1833, 2013.

48. Luchsinger PC, Snell RE, Patel DJ, and Fry DL. Instanteous Pressure Distribution Along the Human Aorta. *Circulation Research* 15: 503-510, 1964.

49. Manini S, Passera K, Huberts W, Botti L, Antiga L, and Remuzzi A. Computational model for simulation of vascular adaptation following vascular access surgery in haemodialysis patients. *Computer Methods In Biomechanics And Biomedical Engineering*, 2013.

50. McGah PM, Leotta DF, Beach KW, Eugene Zierler R, and Aliseda A. Incomplete restoration of homeostatic shear stress within arteriovenous fistulae. *Journal Of Biomechanical Engineering* 135: 011005, 2013.

51. Merillon JP, Motte G, Masquet C, Guiomard A, Baudouy Y, and Gourgon R. [Evaluation of static elasticity and characteristic impedence of the aorta. Their relationships with age, aortic pressure and ventricular ejection resistance]. *Archives Des Maladies Du Coeur Et Des Vaisseaux* 69: 653-659, 1976.

52. Milnor WR. *Hemodynamics*. Baltimore: Williams & Wilkins, 1989.

53. Mohiuddin MW, Laine GA, and Quick CM. Increase in pulse wavelength causes the systemic arterial tree to degenerate into a classical windkessel. *American Journal Of Physiology Heart And Circulatory Physiology* 293: H1164-1171, 2007.

54. Mohiuddin MW, Rihani RJ, Laine GA, and Quick CM. Increasing pulse wave velocity in a realistic cardiovascular model does not increase pulse pressure with age. *American Journal Of Physiology Heart: And Circulatory Physiology* 303: H116-125, 2012.

55. Moreau KL, Silver AE, Dinenno FA, and Seals DR. Habitual aerobic exercise is associated with smaller femoral artery intima-media thickness with age in healthy men and women. *European Journal Of Cardiovascular Prevention And Rehabilitation : Official Journal Of The European Society Of Cardiology, Working Groups On Epidemiology & Prevention And Cardiac Rehabilitation And Exercise Physiology* 13: 805-811, 2006.

56. Moscato F, Wirrmann C, Granegger M, Eskandary F, Zimpfer D, and Schima H. Use of continuous flow ventricular assist devices in patients with heart failure and a normal ejection fraction: a computer-simulation study. *The Journal Of Thoracic And Cardiovascular Surgery* 145: 1352-1358, 2013.

57. Murray CD. The Physiological Principle of Minimum Work: I. The Vascular System and the Cost of Blood Volume. *Proceedings Of The National Academy Of Sciences Of The United States Of America* 12: 207-214, 1926.

58. Nichols WW, Conti CR, Walker WE, and Milnor WR. Input impedance of the systemic circulation in man. *Circulation Research* 40: 451-458, 1977.

59. Nichols WW, Nichols WW, and McDonald DA. *Mcdonald's Blood Flow In Arteries : Theoretic, Experimental, And Clinical Principles*. London: Hodder Arnold, 2011.

60. Ning G, Pan Q, Wang R, Reglin B, Cai G, Yan J, and Pries AR. A One-dimensional Mathematical Model for Studying the Pulsatile Flow in Microvascular Networks. *Journal Of Biomechanical Engineering*, 2013.

61. Noodergraaf A. Hemodynamics. In: *Biological Engineering*, edited by Schwan HP: McGraw-Hill Book Company, 1969, p. 556.

62. Noordergraaf A. *Physical Basis of Ballistocardiography* (Ph.D. Thesis): University of Utrecht, 1956.

63. Noordergraaf A, Verdouw D, and Boom HB. The use of an analog computer in a circulation model. *Progress In Cardiovascular Diseases* 5: 419-439, 1963.

64. Ong CM, Canter CE, Gutierrez FR, Sekarski DR, and Goldring DR. Increased stiffness and persistent narrowing of the aorta after successful repair of coarctation of the aorta: relationship to left ventricular mass and blood pressure at rest and with exercise. *American Heart Journal* 123: 1594-1600, 1992.

65. Oshinski JN, Ku DN, Mukundan S, Jr., Loth F, and Pettigrew RI. Determination of wall shear stress in the aorta with the use of MR phase velocity mapping. *Journal Of Magnetic Resonance Imaging : JMRI* 5: 640-647, 1995.

66. Oyre S, Pedersen EM, Ringgaard S, Boesiger P, and Paaske WP. In vivo wall shear stress measured by magnetic resonance velocity mapping in the normal human abdominal

aorta. *European Journal Of Vascular And Endovascular Surgery : The Official Journal Of The European Society For Vascular Surgery* 13: 263-271, 1997.

67. Pearson AC, Guo R, Orsinelli DA, Binkley PF, and Pasierski TJ. Transesophageal echocardiographic assessment of the effects of age, gender, and hypertension on thoracic aortic wall size, thickness, and stiffness. *American Heart Journal* 128: 344-351, 1994.

68. Pedersen EM, Oyre S, Agerbaek M, Kristensen IB, Ringgaard S, Boesiger P, and Paaske WP. Distribution of early atherosclerotic lesions in the human abdominal aorta correlates with wall shear stresses measured in vivo. *European Journal Of Vascular And Endovascular Surgery : The Official Journal Of The European Society For Vascular Surgery* 18: 328-333, 1999.

69. Piquet L, Dalmay F, Ayoub J, Vandroux JC, Menier R, Antonini MT, and Pourcelot L. Study of blood flow parameters measured in femoral artery after exercise: correlation with maximum oxygen uptake. *Ultrasound In Medicine & Biology* 26: 1001-1007, 2000.

70. Price RJ and Skalak TC. A circumferential stress-growth rule predicts arcade arteriole formation in a network model. *Microcirculation* 2: 41-51, 1995.

71. Pries AR, Reglin B, and Secomb TW. Remodeling of blood vessels: responses of diameter and wall thickness to hemodynamic and metabolic stimuli. *Hypertension* 46: 725-731, 2005.

72. Pries AR, Secomb TW, and Gaehtgens P. Design principles of vascular beds. *Circulation Research* 77: 1017-1023, 1995.

73. Pries AR, Secomb TW, and Gaehtgens P. Structural adaptation and stability of microvascular networks: theory and simulations. *The American Journal Of Physiology* 275: H349-360, 1998.

74. Quick CM, Berger DS, and Noordergraaf A. Apparent arterial compliance. *The American Journal Of Physiology* 274: H1393-1403, 1998.

75. Quick CM, Berger DS, and Noordergraaf A. Constructive and destructive addition of forward and reflected arterial pulse waves. *American Journal Of Physiology Heart And Circulatory Physiology* 280: H1519-1527, 2001.

76. Quick CM, Berger DS, Stewart RH, Laine GA, Hartley CJ, and Noordergraaf A. Resolving the hemodynamic inverse problem. *IEEE Transactions On Bio-Medical Engineering* 53: 361-368, 2006.

77. Quick CM, Leonard EF, and Young WL. Adaptation of cerebral circulation to brain arteriovenous malformations increases feeding artery pressure and decreases regional hypotension. *Neurosurgery* 50: 167-173; discussion 173-165, 2002.

78. Quick CM, Young WL, Leonard EF, Joshi S, Gao E, and Hashimoto T. Model of structural and functional adaptation of small conductance vessels to arterial hypotension. *American Journal Of Physiology: Heart And Circulatory Physiology* 279: H1645-1653, 2000.

79. Quick CM, Young WL, and Noordergraaf A. Infinite number of solutions to the hemodynamic inverse problem. *American Journal Of Physiology: Heart And Circulatory Physiology* 280: H1472-1479, 2001.

80. Remington JW and Wood EH. Formation of peripheral pulse contour in man. *Journal Of Applied Physiology* 9: 433-442, 1956.

81. Reymond P, Bohraus Y, Perren F, Lazeyras F, and Stergiopulos N. Validation of a patient-specific one-dimensional model of the systemic arterial tree. *American Journal Of Physiology Heart And Circulatory Physiology* 301: H1173-1182, 2011.

82. Reymond P, Merenda F, Perren F, Rufenacht D, and Stergiopulos N. Validation of a one-dimensional model of the systemic arterial tree. *American Journal Of Physiology Heart And Circulatory Physiology* 297: H208-222, 2009.

83. Reymond P, Vardoulis O, and Stergiopulos N. Generic and patient-specific models of the arterial tree. *Journal Of Clinical Monitoring And Computing* 26: 375-382, 2012.

84. Rodbard S. Vascular caliber. *Cardiology* 60: 4-49, 1975.

85. Rosen LA, Hollis TM, and Sharma MG. Alterations in bovine endothelial histidine decarboxylase activity following exposure to shearing stresses. *Experimental And Molecular Pathology* 20: 329-343, 1974.

86. Schlager O, Giurgea A, Margeta C, Seidinger D, Steiner-Boeker S, van der Loo B, and Koppensteiner R. Wall shear stress in the superficial femoral artery of healthy adults and its response to postural changes and exercise. *European Journal Of Vascular And Endovascular Surgery : The Official Journal Of The European Society For Vascular Surgery* 41: 821-827, 2011.

87. Shadwick RE. Mechanical design in arteries. *The Journal Of Experimental Biology* 202: 3305-3313, 1999.

88. Shalimova A. [Correction of endothelial dysfunction in patients with essential hypertension and type 2 diabetes]. *Georgian Medical News*: 33-40, 2014.

89. Sluysmans T and Colan SD. Theoretical and empirical derivation of cardiovascular allometric relationships in children. *J Appl Physiol (1985)* 99: 445-457, 2005.

90. Sonesson B, Hansen F, Stale H, and Lanne T. Compliance and diameter in the human abdominal aorta--the influence of age and sex. *European Journal Of Vascular Surgery* 7: 690-697, 1993.

91. Stefanadis C, Stratos C, Boudoulas H, Kourouklis C, and Toutouzas P. Distensibility of the ascending aorta: comparison of invasive and non-invasive techniques in healthy men and in men with coronary artery disease. *European Heart Journal* 11: 990-996, 1990.

92. Stergiopulos N, Meister JJ, and Westerhof N. Evaluation of methods for estimation of total arterial compliance. *The American Journal Of Physiology* 268: H1540-1548, 1995.

93. Stergiopulos N, Young DF, and Rogge TR. Computer simulation of arterial flow with applications to arterial and aortic stenoses. *Journal Of Biomechanics* 25: 1477-1488, 1992.

94. Sweitzer NK, Shenoy M, Stein JH, Keles S, Palta M, LeCaire T, and Mitchell GF. Increases in central aortic impedance precede alterations in arterial stiffness measures in type 1 diabetes. *Diabetes Care* 30: 2886-2891, 2007.

95. Tang BT, Cheng CP, Draney MT, Wilson NM, Tsao PS, Herfkens RJ, and Taylor CA. Abdominal aortic hemodynamics in young healthy adults at rest and during lower

limb exercise: quantification using image-based computer modeling. *American Journal Of Physiology Heart And Circulatory Physiology* 291: H668-676, 2006.

96. Temmar M, Jankowski P, Peltier M, Mouquet V, Debicka-Dabrowska D, Hamida F, Kawecka-Jaszcz K, and Safar ME. Intraaortic pulse pressure amplification in subjects at high coronary risk. *Hypertension* 55: 327-332, 2010.

97. Templeton DL, John R, Painter P, Kelly AS, and Dengel DR. Effects of the left ventricular assist device on the compliance and distensibility of the carotid artery. *Heart And Vessels* 28: 377-384, 2013.

98. Thulesius O and Lanne T. The importance of arterial compliance for the determination of ankle systolic pressure. *VASA Zeitschrift Fur Gefasskrankheiten* 16: 270-273, 1987.

99. Travis AR, Giridharan GA, Pantalos GM, Dowling RD, Prabhu SD, Slaughter MS, Sobieski M, Undar A, Farrar DJ, and Koenig SC. Vascular pulsatility in patients with a pulsatile- or continuous-flow ventricular assist device. *The Journal Of Thoracic And Cardiovascular Surgery* 133: 517-524, 2007.

100. Tsamis A, Rachev A, and Stergiopulos N. A constituent-based model of age-related changes in conduit arteries. *American Journal Of Physiology Heart And Circulatory Physiology* 301: H1286-1301, 2011.

101. Tsamis A, Stergiopulos N, and Rachev A. A structure-based model of arterial remodeling in response to sustained hypertension. *Journal Of Biomechanical Engineering* 131: 101004, 2009.

102. VanNess JM, Casto RM, and Overton JM. Antihypertensive effects of food-intake restriction in aortic coarctation hypertension. *Journal Of Hypertension* 15: 1253-1262, 1997.

103. Vita JA, Holbrook M, Palmisano J, Shenouda SM, Chung WB, Hamburg NM, Eskenazi BR, Joseph L, and Shapira OM. Flow-induced arterial remodeling relates to endothelial function in the human forearm. *Circulation* 117: 3126-3133, 2008.

104. Wang Y, Loghmanpour N, Vandenberghe S, Ferreira A, Keller B, Gorcsan J, and Antaki J. Simulation of dilated heart failure with continuous flow circulatory support. *PloS one* 9: e85234, 2014.

105. Wells SM, Langille BL, and Adamson SL. In vivo and in vitro mechanical properties of the sheep thoracic aorta in the perinatal period and adulthood. *The American Journal Of Physiology* 274: H1749-1760, 1998.

106. West GB, Brown JH, and Enquist BJ. A general model for the origin of allometric scaling laws in biology. *Science* 276: 122-126, 1997.

107. Westerhof N, Bosman F, De Vries CJ, and Noordergraaf A. Analog studies of the human systemic arterial tree. *Journal Of Biomechanics* 2: 121-143, 1969.

108. White CR and Seymour RS. Allometric scaling of mammalian metabolism. *The Journal Of Experimental Biology* 208: 1611-1619, 2005.

109. Wolinsky H and Glagov S. Nature of species differences in the medial distribution of aortic vasa vasorum in mammals. *Circulation Research* 20: 409-421, 1967.

110. Womersley JR. Oscillatory flow in arteries. II. The reflection of the pulse wave at junctions and rigid inserts in the arterial system. *Physics In Medicine And Biology* 2: 313-323, 1958.

111. Xiao N, Humphrey JD, and Figueroa CA. Multi-Scale Computational Model of Three-Dimensional Hemodynamics within a Deformable Full-Body Arterial Network. *Journal Of Computational Physics* 244: 22-40, 2013.

112. Zamir M. Shear forces and blood vessel radii in the cardiovascular system. *The Journal Of General Physiology* 69: 449-461, 1977.

113. Zwolak RM, Adams MC, and Clowes AW. Kinetics of vein graft hyperplasia: association with tangential stress. *Journal Of Vascular Surgery* 5: 126-136, 1987.